Univerzita Karlova v Praze

Matematicko-fyzikální fakulta

DIPLOMOVÁ PRÁCE

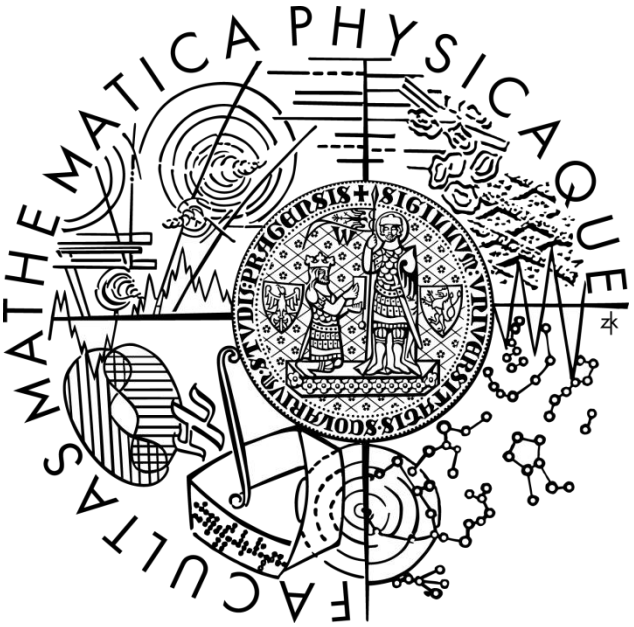

Petr Čermák

Studium magnetických vlastností sloučenin ceru pomocí tepelné kapacity

Katedra fyziky kondenzovaných látek

Vedoucí diplomové práce: *doc. Mgr. Pavel Javorský, Dr.*

Studijní program: *Fyzika, FKSM*
fyzika kondenzovaných soustav a materiálů

Charles University in Prague
Faculty of Mathematics and Physics

DIPLOMA THESIS

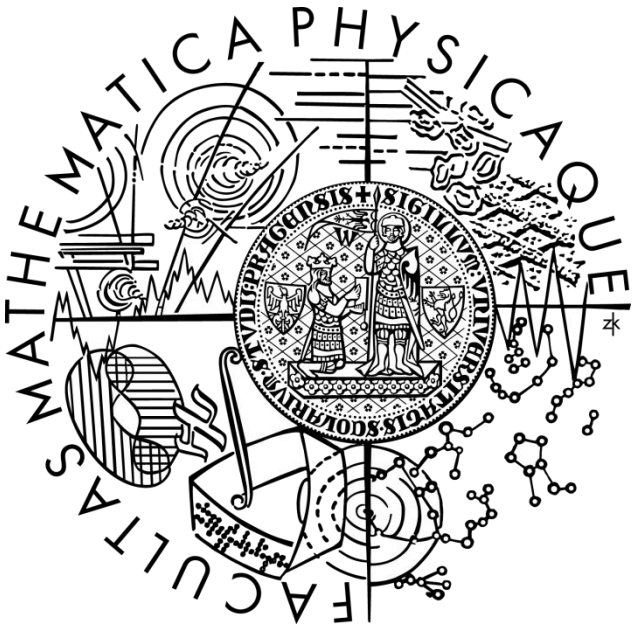

Petr Čermák

Magnetic properties of Ce compounds studied by specific heat

Department of Condensed Matter Physics

Supervisor: *doc. Mgr. Pavel Javorský, Dr.*

Study program: *Physics,*
Physics of Condensed Matter and Materials

Poděkování

Velmi rád bych poděkoval a vyslovil uznání všem, kteří mi pomáhali při vzniku této práce. Především doc. Pavlu Javorskému, Dr., vedoucímu mé diplomové práce, za trpělivé vedení a množství praktických rad. Doc. Javorský mi poskytl zázemí potřebné pro vznik celé práce a velmi mi pomohl svými znalostmi i prostředky. Dále Mgr. Kláře Uhlířové, mé konzultantce, která mi vždy ochotně pomohla cennými informacemi a svými zkušenostmi. Dále také RNDr. Jiřímu Prchalovi, Ph.D. za pomoc s interpretací dat z polních měření a RNDr. Stanislavu Danišovi, Ph.D. za pomoc s programem Fullprof.

Rovněž děkuji RNDr. Evě Šantavé, CSc. za laskavou pomoc při obsluhování měřící aparatury PPMS. Dále také děkuji Dr. Andreasu Hoserovi a Dr. Tommymu Hofmannovi za jejich čas a pomoc s mým experimentem na neutronovém zdroji v Berlíně.

Nakonec bych chtěl poděkovat rodičům za poskytnuté zázemí a své milované přítelkyni za její trpělivost a lásku.

Prohlašuji, že jsem svou diplomovou práci napsal(a) samostatně a výhradně s použitím citovaných pramenů. Souhlasím se zapůjčováním práce.

V Praze dne 16. 4. 2010 Petr Čermák

Contents

Název práce: *Studium magnetických vlastností sloučenin ceru pomocí tepelné kapacity*
Autor: *Petr Čermák*
Katedra (ústav): *Katedra fyziky kondenzovaných látek*
Vedoucí diplomové práce: *doc. Mgr. Pavel Javorský, Dr.*
e-mail vedoucího: *javor@mag.mff.cuni.cz*

Abstrakt: *Látky obsahující 4f (vzácné zeminy) nebo 5f (aktinoidy) vykazují širokou škálu zajímavých fyzikálních vlastností. Mezi sloučeninami vzácných zemin mají zvláštní postavení sloučeniny ceru. Atom ceru obsahuje pouze jediný f-elektron, zodpovědný za magnetické chování. Na rozdíl od látek obsahujících těžké vzácné zeminy, u nichž mají 4f elektronové stavy lokalizovanou povahu, se mnohé cerové sloučeniny nachází na hranici mezi itinerantním a lokalizovaným chováním. Výsledkem soupeření mezi dalekodosahovým uspořádáním zpravidla typu RKKY a stínění lokalizovaných momentů vodivostními elektrony je široká škála elektronových a magnetických základních stavů těchto sloučenin od nemagnetických se smíšenou valencí (tj. valence iontu ceru fluktuuje mezi Ce^{3+} a Ce^{4+}) až po kovové systémy s dalekodosahovým uspořádáním magnetických momentů ceru v základním stavu (kde se může jednat o feromagnetické, antiferomagnetické nebo i složitější magnetické uspořádání). Nezastupitelnou úlohu při studiu chování těchto látek má přitom znalost experimentálních dat tepelné kapacity, zejména nízkoteplotní části.*
Náplní práce je příprava vybraných cerových intermetalických vzorků, jejich fázová charakteristika a především měření tepelné kapacity při nízkých teplotách (0.4 - 300 K). Značná část práce je věnována analýze naměřených dat a jejich srovnání s teoretickými modely.
Klíčová slova: *cer, tepelná kapacita, intermetalika*

Title: *Magnetic properties of Ce compounds studied by specific heat*
Author: *Petr Čermák*
Department: *Department of Condensed Matter Physics*
Supervisor: *doc. Mgr. Pavel Javorský, Dr.*
Supervisor's e-mail address: *javor@mag.mff.cuni.cz*

Abstract: *Materials containing the 4f (rare earth) or 5f (actinides) exhibit a large variety of interesting physical properties. The Ce-based compounds have a special place among the rare-earth compounds. The Ce atom contains only a single f-electron that is responsible for the magnetic behavior. The 4f states in compounds with the heavy rare earths have a well localized character, whereas many Ce-based compounds are on the borderline between the localized and itinerant behavior. These compounds show large variety of the magnetic ground states what is a result of the competition between the long-range order of the RKKY type and the screening of the localized moments by conduction electrons. We observe nonmagnetic states with a mixed valence (between Ce^{3+} and Ce^{4+}), metallic systems with a long-range order of the Ce moments (ferromagnetic, antiferromagnetic or more complex structures). To analyze the electronic properties, the heat capacity data, and namely their low-temperature part, play an indispensable role.*
This diploma work comprise the sample preparation of selected cerium compounds, their phase characteristics and the heat capacity measurements at low temperatures (0.4 - 300 K). The main part is focused on the data analysis and comparison with theoretical models.
Keywords: *cerium, heat capacity, intermetalics*

1. Introduction

Recent discoveries of new materials and improved calorimetric techniques increase importance of specific heat measurements. Several companies (Quantum design, Anter Corp, Cryogenic Ltd.) sell commercial instruments capable of a precise and accurate measurement of temperature dependence of the specific heat in a quite large temperature range. These are the main reasons, why is the specific heat study becoming a standard research tool.

In principle, any temperature-dependent phenomenon can contribute to the specific heat of a system since it affects the energy level of particles or modes that determine the mean energy. These levels may arise from translation, rotation or vibration motion of the atoms or molecules, or from electronic or spin excitations and so on. Hence the subject of specific heat covers a very broad field like phonon vibrations, nuclear-electron interactions and especially ordering of any kind. It is useful method for revealing microscopic changes in a material with only bulk measurement.

Described advantages are also the main disadvantages. There are many additive contributions to the specific heat but only total heat capacity can be experimentally measured. Separation of single contributions is the most difficult task in the specific-heat evaluation. Therefore it is not possible to describe or study only selected contributions to the specific heat which are interesting for given measurement. Every time we must count on all possible contributions. In many publications is the examination of the specific heat limited to only electron and phonon contributions neglecting for example Schottky specific heat. This consecution can lead to a misinterpretation of measured data.

Purpose of this work is to systematically describe detailed evaluation of total specific heat in broad temperature range (0.5~300K) with accent on correct separation of specific heat contributions. All techniques will be described on real samples which belong to “hot-topics” in present science.

For this detailed analysis of the specific heat we choose to study cerium compounds. Many scientists declare that Ce (together with Pu) in its elemental form and also its intermetallic alloys are the most fascinating materials in condensed matter physics [1] [2]. On these compounds we can observe magnetic ordering, metamagnetic transitions and also non-magnetic ground state. Many of these compounds reveal heavy fermion behavior, Kondo effect, unconventional superconductivity, mixed valence state and other.

Cerium compounds are large unexplored playground on which we can watch a lot of different aspects of modern condensed matter physics.

1.1. Outline

The main subject of this work is a systematic study of specific heat methods showed on variety of cerium compounds. The theory of specific heat and main aspects of Cerium compounds are briefly summarized in Chapter 2. These theoretical concepts go beyond the topic of the thesis, but it is necessary to know it. Studied materials have been already investigated in many publications. All previous results together with brief overview off all studied samples are described in Chapter 3. All sample measurements, preparation techniques and results are segmented by studied material in Chapter 4.

2. Theory

2.1. Rare earth magnetism

Rare-earth metals reveal different type of magnetism than other metals and form its own branch of the solid state physics. Carriers of magnetism in rare earths are strongly localized electrons in 4f shell. This shell fills with electrons gradually from ^{57}La to ^{71}Lu. Most important property of the 4f-orbitals is their radius which is about 10 times smaller than the minimum inter-atomic distance in solid. This forbids any direct f-f exchange interaction, so indirect interaction mediated by conduction electrons – called *RKKY* – raised in importance. It is long-range interaction with oscillating character.

Charge distribution around an ion produces an electric field, called *crystal field*. This field acts on electrons in 4f shell, giving rise to the strong magnetic anisotropy of rare earths materials. In a view of one atom, crystal field removes directional degeneracy reflecting the symmetry of nearby atoms. Splitting of the terms depends on the crystal field symmetry. Generally we can say, that with lower symmetry splitting increases.

As said above, 4f electrons are hidden deep inside an ion, so they are not much influenced by the crystal field. This implies separation of spin-orbit coupling (energies in order of 100 meV) and crystal field splitting. Typical crystal field splitting in rare earths correspond to energies about 10 meV, in temperature range it is hundreds of Kelvins.

Calculation of crystal field is possible from first principles. For described system with weak crystal field, we can express crystal field Hamiltonian with simple relationship:

$$\hat{\mathcal{H}}_{CF} = \sum_{lm} B_l^m \hat{O}_l^m . \tag{1}$$

B_l^m are crystal field parameters which can be calculated from a point charge model if we know exact structure of the compound. Else it can be determined experimentally. $\hat{O}_l^m$ are Steven's operators representing the whole 4f shell (see [3] for details). Number of independent parameters in B_l^m matrix depends on the symmetry of the crystal field. For example cubic symmetry have only two independent crystal field parameters B_4 and B_6, while for orthorhombic structure there are 9 independent parameters.

For cerium atoms, there is another important phenomenon, which influence ground state of the ion. There exists a coupling between 4f and conduction electrons - *Kondo effect*. It is a many body problem, with a lot of theoretical approaches. Theories define Kondo temperature T_K as the energy scale limiting validity of the Kondo results. Under this temperature magnetic moment of the 4f electron and conduction electron moment binds together. But there exists another interaction between 4f and conduction electrons – RKKY, which often causes ferromagnetic or antiferromagnetic ordering. In case of antiferromagnetic RKKY ordering, Kondo effect acts contrary to it. This interplay can be described by the Doniach diagram – graphical representation of Kondo and Néel temperature dependence on exchange constant J.

Mostly we found cerium in trivalent state in a numbers of ferromagnetic and antiferromagnetic compounds. Hybridization between the 4f electron orbitals and conduction

electrons can lead to hopping of electrons between f^0 and f^1 states. This corresponds to dynamic distribution of Ce^{3+} and Ce^{4+} ions over lattice. This situation is called *mixed valence*.

2.2. Heat capacity

Specific heat is originally thermodynamic quantity, revealing the amount of heat required to raise the temperature of a unit mass by a temperature unit degree. This basic definition can by expressed by the equation

$$C_x(T) = \left(\frac{dQ}{dT}\right)_x, \tag{2}$$

where x is a thermodynamic parameter which remains constant during a measurement. From experimental point of view x is usually pressure, which is kept constant for most bulk measurements. Important point for practical measurement is that equation (2) is valid only in thermodynamic equilibrium, so $dT \ll T$.

Described definition is useful for specifying general laws in thermodynamics. For retrieving some information from microscopic structure of our sample it is desirable to modify it to form

$$C_V = -T\left(\frac{\partial^2 F}{\partial T^2}\right)_V. \tag{3}$$

Here F is Helmholtz free energy, which is equal to the maximum amount of work extractable from a thermodynamic process with constant volume V. With application of statistical mechanic laws, it is possible to retrieve another useful definition of the specific heat via entropy S:

$$C_V = T\left(\frac{\partial S}{\partial T}\right)_V \tag{4}$$

As one can see from (3) and (4) specific heat is tightly bind to total free energy and to amount of order in the sample. Every physical phenomenon, which changes energy levels of particles in material, will contribute to its specific heat. Existence of bulk measurement reflecting microscopic changes in sample is very useful, but brings also some difficulties. Main problem is impossibility of experimental differentiating sources of measured specific heat. Total free energy of system is a sum of the free energies of its components so that the total specific heat is the sum of these contributions – see (3).

Idea of extracting individual contributions is based on choosing temperature range, where is one of these contributions dominant. The largest contribution to C gives us lattice vibrations (phonons) - C_{ph}. In conductive samples is always present electronic contribution C_{el} due to conduction electrons. Magnetic samples have additional contributions, discussed below. The only contribution, which will not be discussed and measured, is nuclear contribution C_N.

All formulas express specific heat measured with constant volume. But in real experiments, we measure with constant pressure C_p. So for analysis C_p versus T data it is

necessary to convert C_p to C_V. The most common procedure is to use the well known thermodynamic relation

$$C_V = C_p - \alpha_V^2 \frac{TV}{\beta_T}. \tag{5}$$

However α_V (thermal expansion coefficient) and β_T (compressibility) are rarely available data, mostly dependent on temperature and in a non-cubic case they are second-rank tensors. So it is impossible to use this equation in real experiments. Other alternatives will be discussed below.

2.2.1. Phonon specific heat

This contribution is caused by thermal lattice vibrations. It is present in all compounds and generates largest part of the total specific heat. The first specific heat equation - Dulong-Petit law $C_{ph} = 3\mathrm{N_A k_B}$ was about phonon specific heat. Nowadays it is well known, that this equation is not true, it is approximately valid only in high temperatures (around 300K). The phonon specific heat then decreases with decreasing temperature down to zero at 0 K. Invalidity of Dulong-petit relationship was one of the first impulses leading to quantum physics of solids.

Consider a model of N independent atoms oscillating in parabolic potential. It will act as N linear harmonic oscillators and overall energy of lattice can be calculated as:

$$E_{ph} = \sum_{j=1}^{3N} \left(n_j + \frac{1}{2}\right) \mathrm{h}\nu_j \qquad n = 0,1,2 \ldots \tag{6}$$

where $\mathrm{h}\nu_j$ is energy quantum of lattice vibration, commonly called phonon. To calculate specific heat from this equation, we must know phonon frequency spectra of the lattice. However exact calculation of frequency spectra for real material is very difficult, so we must make some approximations.

For simplicity consider infinite repeating chain of m different atoms. Restrict interactions only to nearest neighborhood and assume elastic forces. Then we obtain system of linear homogenous equations leading to m frequency spectra $\omega_i(k)$. One of these frequencies is almost directly proportional to wave vector k. This $\omega(k)$ is called acoustic branch of phonon spectra because of parallel with sound waves. Remaining $m-1$ branches are nearly constant with wave vector and are denoted as optical branches. Expansion of this theory to the three-dimensional case leads to 3 acoustic branches and $3(p-1)$ optical branches.

The Einstein model is suitable for describing optical branches. It presumes that all atoms oscillate on the same frequency ω_E. Specific heat for one optical branch is expressed by form:

$$C_E = 3\mathrm{k_B N_A} \left(\frac{\theta_E}{T}\right)^2 \frac{\left(e^{\theta_E/T}\right)}{(e^{\theta_E/T}-1)^2}, \qquad \theta_E = \frac{h\omega_E}{k_B}, \tag{7}$$

where θ_E is Einstein temperature characterizing one branch.

Situation is different in acoustic branches, where Debey theory is used. It presumes elastic dispersion of oscillations (like sound waves). Calculation of specific heat for all three acoustic branches is then more complex and leads to following formula for one acoustic branch:

$$C_D = 3\mathrm{k_b N_A}\left(\frac{T}{\theta_D}\right)^3 \int_0^{\frac{\theta_D}{T}} \frac{x^4 e^x}{(e^x-1)^2}\,dx, \tag{8}$$

where θ_D is Debye temperature characterizing branch. Overall phonon contribution is then sum of contributions for each branch and it is dependent on $3p$ independent variables.

All these theories are based on harmonic approximation of the lattice dynamics. Corrections due to the anharmonic cubic and quadratic terms are extremely difficult to evaluate, but quantitatively they add a linear temperature term to C_V at high temperatures. These corrections are very small perturbations compared to perturbations due to thermal expansion, see *(5)*. Taking into account thermal expansion, we can correct (7) and (8) with anharmonic terms [4] and overall phonon specific heat will be

$$C_{ph} = \frac{1}{1-\alpha_D T} C_D + \sum_{i=1}^{3p-3} \frac{1}{1-\alpha_{Ei} T} C_{Ei} \tag{9}$$

where α_D and α_{Ei} are anharmonic coefficients. Totally we gain equation with $6p-4$ independent variables for only phonon specific heat contribution. These parameters forms very unstable system for real materials, which makes fitting indeed impossible. Therefore we obviously group the branches together to some kind of a degenerated branches reducing number of independent variables. Generally we can assume, that compounds with similar lattice parameters will have similar ω dependencies on k, which means similar phonon specific heat contributions.

In the low temperature range ($T \lesssim \frac{\theta_D}{20}$) dominates acoustic branches and the phonon contribution could be well done expressed with only Debye formula (8). The Debye integral can be approximated with a third order polynomial [2]. So the phonon contribution in the low temperatures is given by

$$C_{ph} = \beta T^3, \tag{10}$$

where $\beta = \frac{12}{5}\pi^4 R\left(\frac{1}{\theta_D}\right)^3$.

2.2.2. Electron specific heat

In compounds with conduction electrons, we have another contribution to the total specific heat. Mostly used theory comes from free electron gas model with Fermi-Dirac distribution. Fundamental on this theory is that only electrons near Fermi level will excite to higher energy levels. Number of these electrons is proportional to the T/T_F rate. This assumption is valid only for temperatures much smaller than Fermi temperature (T_F), which means valid in temperature range where metals are in a solid state.

These excited electrons gain energy of the order of $k_B T$, so overall electronic kinetic energy is proportional to T^2. While heat capacity is first derivative of energy, we gain simple assumption that electronic specific heat depends linear on a temperature. Exact formula [5] is

$$C_{el} = \frac{1}{3}\pi^2 \mathcal{D}(E_F) \mathrm{k_B}^2 T = \gamma T \tag{11}$$

where $\mathcal{D}(E_F)$ is the density of electronic states at the Fermi energy, γ is Sommerfeld coefficient or Sommerfeld electronic factor and characterizes proportionality constant between electron specific heat and temperature.

There should be noted, that γ-factor determined from specific heat measurement:

$$\gamma = \frac{C_{el}}{T} \tag{12}$$

could be different from the Sommerfeld coefficient from (11). The differences arise from electron-phonon (*e-ph*) and electron-magnon (*e-mag*) interactions and expose in another specific heat contribution linearly dependent on temperature. These contributions are often grouped with conduction electron specific heat and in simple case only renormalize Sommerfeld coefficient value:

$$\gamma = \gamma_0 \left(1 + \lambda_{e-ph} + \lambda_{e-mag}\right). \tag{13}$$

Here λ's are coefficients related to added interactions, γ_0 is Sommerfeld coefficient from (11) and γ is constant from (12). In literature is frequently called Sommerfeld coefficient, which is not accurate.

2.2.3. Schottky paramagnetic contribution

The crystal field plays an important role in the formation of the ground states of the lanthanides. Ions of rare-earths are exposed to electrostatic field from surrounding ions and electrons – crystal field. This field can split ground state energy level of the ion. These energy levels can be obtained from diagonalization of the Hamiltonian $\mathcal{H}_{CF}$ in (1) so ab initio calculation can be used. For experimental application is useful important phenomenon – Kramers theorem. It states that the energy levels of systems with an odd number of electrons remain at least doubly degenerate in the presence of purely electric fields (what means no external magnetic fields) and remains valid independently on crystal field symmetry.

The energy levels are preferably determined from inelastic thermal neutron scattering. Thermal neutrons have energies comparable with the energy levels and can cause excitations.

Splitting of degenerated ground state brings increase of entropy and related specific heat contribution. This contribution is often called Schottky specific heat C_{sch} and from statistical physics we can obtain following relation:

$$C_{sch} = \mathrm{k_B N_A} \left(\frac{\sum_{i=1}^{n} \left(\frac{E_i}{\mathrm{k_B}T}\right)^2 e^{-\frac{E_i}{\mathrm{k_B}T}}}{\sum_{i=1}^{n} e^{-\frac{E_i}{\mathrm{k_B}T}}} - \left(\frac{\sum_{i=1}^{n} \frac{E_i}{\mathrm{k_B}T} e^{-\frac{E_i}{\mathrm{k_B}T}}}{\sum_{i=1}^{n} e^{-\frac{E_i}{\mathrm{k_B}T}}} \right)^2 \right) \tag{14}$$

where n is the number of energy levels and E_i is energy of the level.

We can simply calculate the total amount of the entropy connected with the crystal field splitting as

$$\Delta S = R \ln n. \tag{15}$$

From the Hund rules the total angular momentum of Ce^{3+} is $J = \frac{5}{2}$, with a degeneracy of $2J + 1 = 6$. The CF splits this degeneracy into a doublet and a quartet in a cubic symmetry and into three Kramer doublets in a lower symmetry. This quite simple CF level scheme of Ce^{3+} allows us to describe Schottky contribution with two independent parameters.

2.2.4. Specific heat related to magnetic order

In a magnetic system we must add another contribution to total specific heat connected with magnetic order – C_M. In practice electron and phonon contribution is subtracted from measured specific heat to obtain only magnetic contribution:

$$C_M = C_p - \left(C_{el} + C_{ph} + C_{sch}\right). \tag{16}$$

Nonmagnetic contributions can be obtained from fitting specific heat data at higher temperatures, which is often difficult, or from a reference nonmagnetic compound, usually formed with La, Y or Lu instead of rare earth magnetic on.

C_M shows another linear contribution at some range of temperature for most of Ce compounds [2]. It has also electronic origin, but does not necessarily represent a density of states as γ does. Therefore we can define γ_{LT} and γ_{HT} as C_M/T ratio at low temperature and high temperature region. γ_{HT} is also known as γ_p - the paramagnetic Sommerfeld coefficient γ.

The main part of C_M originates from localized 4f electrons in case of rare earth metals. These electrons are responsible for the magnetic order. From a thermodynamical point of view is magnetic order most often 2nd order phase transition and it is presented as a discontinuity in specific heat. 1st order phase transition will be presented as an entropy discontinuity. Ordering temperature is called a Néel temperature T_N for antiferromagneticaly ordered compounds and Curie temperature T_C for ferromagneticaly ordered compounds. Most of Ce compounds have a doublet as a crystal field ground state, thus the entropy gain associated with their magnetic phase transition is expected as

$$\Delta S = R \ln 2. \tag{17}$$

In a graphical representation ΔS means the area of the phase transition peak in $C/T\ (T)$ dependence. Mean-field theory also predicts height of this peak $\Delta C_M = 1.5R$ for a typical cerium compound with $J = \frac{1}{2}$ ground state. In real samples this value is only a theoretical upper limit, because of magnetic excitations above T_0.

At $T < T_{ord}$ region, $C_M(T)$ is described by magnetic spin waves theory. A number of theories were created based on calculation magnon dispersion relation [6]. Spin wave theory for a simple ferro- and ferrimagnet gives a quadratic magnon dispersion relation at very low temperatures in the long wave-length limit. According to this theory $C_M \sim T^{3/2}$. Do not

mistake with Bloch $T^{3/2}$ law. For simple 3D antiferromagnetic compounds spin wave theory gives a linear magnon dispersion relation and $C_M \sim T^3$.

Additionally, the magnetic anisotropy arising from the molecular fields will introduce a finite gap in the magnon dispersion curve. Thus it modifies mentioned formulas with a factor $\exp(-\delta/T)$, where δ is temperature related to size of the gap .

We can summarize all mentioned simple cases supplemented with dimension calculation to a formula:

$$C_M \sim T^{\frac{d}{m}} \exp\left(-\frac{\delta}{T}\right) \tag{18}$$

where d is dimensionality of magnon excitations and m is defined as the exponent in the dispersion relation $\omega \sim k^m$. For antiferromagnetic magnons $m = 1$ and for ferromagnetic $m = 2$.

There must be noted that described expressions are valid only for simple magnetic models. Application to the real structures with unknown magnetic structure may lead to misinterpretation of fitted parameters.

2.2.5. Kondo effect

If calculated area of the phase transition peak does not reach the theoretical value from (17), it could involve more complex magnetic properties like the Kondo behavior.

Originally is the Kondo effect applicable to metallic systems with a very small amount of magnetic impurities. These impurities are isolated and experience only mild antiferromagnetic correlations in the vicinity of the impurity. As the temperature decreases to zero, the impurity magnetic moment and one conduction electron moment bind very strongly to form an overall non-magnetic state with increased resistivity. Thus we can observe minima in resistivity at low temperatures. If we raise number of the impurities, they start interact with each other via conductive electrons (RKKY interaction) and it destroys Kondo behavior.

The minimum in resistivity is also observed in certain rare-earth non-dilute compounds, especially those with cerium or ytterbium, and Kondo theory can be also applied here. These types of compounds are generally known as heavy fermion systems because the scattering of the conduction electrons with magnetic ions results in a strongly enhanced effective mass (which means very high γ-value in (11)). Nowadays the Kondo effect is general name for many-body problem of localized magnetic moments interacting with conduction electrons in a metal. It is usually indicated with a logarithmic increase in the resistivity at low temperatures.

The strange point is that Kondo interactions act against magnetic ordering (caused by RKKY interaction as described in 2.1). This interplay can be best shown on the *Doniach diagram* (Fig. 1) where ordering and Kondo temperatures as a function of the exchange constant J are plotted. RKKY interaction is higher than Kondo interaction for small $|JN(E_F)|$ values. The system goes then directly from paramagnetic state to magnetic phase with localized moments. On the other hand, for large $|JN(E_F)|$ values Kondo temperature is higher than ordering temperature and localized moments in these systems will be compensated by Kondo interaction before system reaches ordered state. Red line represents the real ordering temperature T_N. Interesting point is where T_N reaches 0 which corresponds to quantum critical

point (QCP) between Kondo singlet and RKKY magnetic ground state. The approach to the QCP is connected with many interesting effects and it is not yet satisfactorily described.

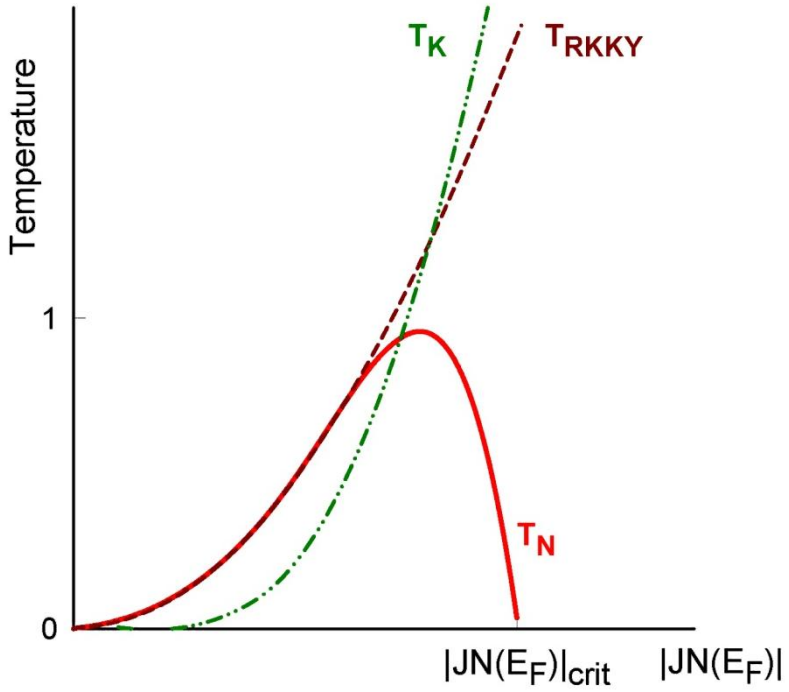

Fig. 1 – Doniach phase diagram

The Kondo effect will influence also the specific heat by reducing the magnetic entropy. The equation (17) is then not valid and the entropy is smaller than the theoretical value. There are lots of detailed theoretical models applicable for different compounds, but we want to have only one simple model for comparing it on different compounds. We presume simple two-level model with an energy splitting of $k_B T_K$, where T_K is the Kondo temperature characterizing Kondo behavior in a given compound. We can estimate Kondo temperature if we can deduce the reduced magnetic entropy ΔS_0 at T_{ord} [7]:

$$\frac{\Delta S_0}{R} = \ln(1+\kappa) + \frac{T_K}{T_{ord}}\left(\frac{\kappa}{1+\kappa}\right) \qquad \kappa = \exp\left(\frac{-T_K}{T_{ord}}\right) \tag{19}$$

We counts only with simple Kondo model, so obtained Kondo temperature may be different from temperatures deduced from other methods or experiments. Nevertheless obtained trends in series of compounds will be qualitatively valid and useful for understanding magnetic development across the series.

2.3. Mixed valence

Certain rare-earth elements (cerium, samarium) reveal a special state of matter called mixed valence (sometimes noted as intermediate or also hybrid valence). These compounds have very large hybridization between the conduction electron states and the 4f electron states. This hybridization causes overlapping of these states and there can be charge transfer between two levels. Ce-ions have this specific behavior because the cerium valence can change from trivalent to tetravalent. Mostly it is indicated by a broad shallow maximum in magnetic susceptibility.

For weaker hybridization the charge fluctuation may not be possible. There can occur spin fluctuations, which will lead to Kondo behavior.

2.4. Solution growth

Many materials, especially rare earth intermetallics, show a strong anisotropy of their electronic properties. Therefore, it is paid a lot of effort to grow single-crystalline samples, which have in addition higher level of purity. Single crystals can be prepared by a large variety of techniques. We can classify them accordingly to three main principles: *growth from the melt* [8] (Czochralski method – well known from silicon industry, Bridgman technique, Zone melting technique – using electron beam, radio-frequency induction or mirror furnace [9]), *growth from the vapor phase* [8] and *growth from solution* [8] [10] [11] [12].

To explain the principle of the solution growth method, let's use an example of growing an incongruently melting compound AlU_3 from Al rich solution (Al flux). The temperature-composition phase diagram for U and Al is presented in Fig. 2. According to this diagram the starting composition should be between 3-15% of U. From U richer composition unwanted phase UAl_2 would grow as well. The starting composition of UAl_9 is chosen in our example and it is heated to 1400°C (point A). Then the cooling of the melt begins with a slow constant rate. At the temperature 1180°C (point B) the solution reaches the solidus-liquidus line. Single crystals of UAl_3 start to grow while the solution becomes Al richer, following the composition at the liquidus line. To avoid UAl_4 phase, the cooling should be stopped above 730 °C, peritetic point of UAl_4). Then, the remaining flux can be decanted by a standard way [11]. In some cases etching is used instead of decanting the remaining flux.

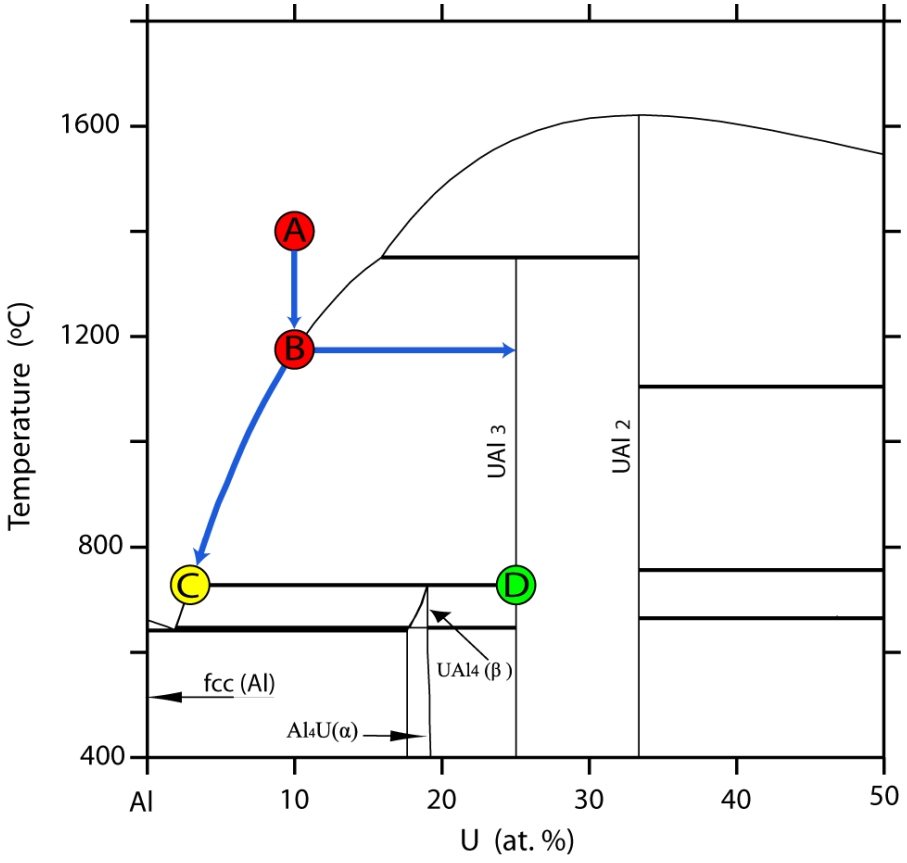

Fig. 2 – The U-Al binary phase diagram [13]

The situation is more complicated, when the temperature-composition phase diagram is not known or incomplete, which is the case of ternary or even more complicated compounds. Searching for proper solvent, optimal starting composition and thermal process is usually the central complex problem of the solution growth method.

2.5. Specific heat measurement

All specific heat measurements were done in the Joint laboratory for magnetic studies (JLMS) on Physical Property Measurement System (PPMS) from Quantum Design. This instrument measures the heat capacity at constant pressure C_p with a relaxation method.

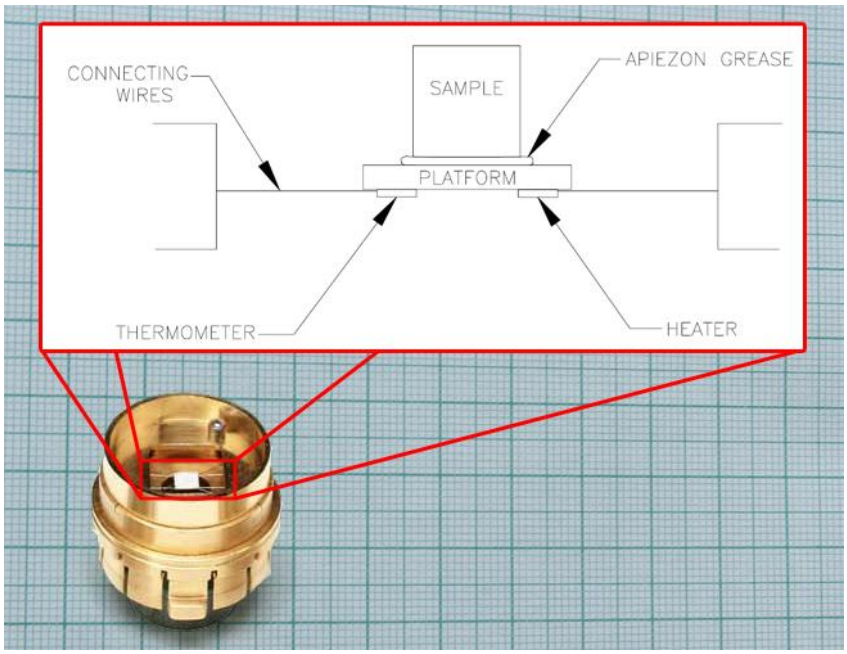

Fig. 3 – Calorimeter puck

During measurement of a one point a known amount of heat is applied at constant power P for a fixed time with a heater (refer Fig. 3). This heating period is followed by a cooling period of the same or longer duration. Small wires provide the electrical and thermal connection to the platform. The sample is mounted to the platform using a thin layer of special grease called Apizeon, which provides the required thermal contact even at low temperatures. Calorimeter puck is placed into a high vacuum PPMS cryostat, surrounded with magnets for application of an external magnetic field.

After each measurement cycle the Quantum Design software fits the entire temperature response of the whole sample platform. There are two possible models. *Simple model* assume, that the sample holder and the sample are in a perfect thermal contact, which means that they are at the same temperature during the measurement. This model measures total heat capacity of sample and platform - C_{total} . It uses basic definition of heat capacity which means energy needed to increase temperature of a material by one unit. Accordingly we can build following differential equation:

$$C_{total}\frac{dT}{dt} = P(t) - K_w(T - T_b), \tag{20}$$

where $P(t)$ is the power applied by the heater, T is a temperature of the platform and t is time. Second term is added to express heat loss between platform and the puck. K_w is the thermal conductance of the supporting wires and T_B is the temperature of the puck frame. Thus applied power is constant in heating period and zero in cooling period, solving this equation is very easy. The solution is given by exponential function, with a characteristic constant C_{total}/K_W (called time constant τ in PPMS software).

Fitting of measured $T(t)$ dependence to this solution gives us C_{total}. But we want only heat capacity of the sample, so we must substract heat capacity of the platform $C_{platform}$ (called addenda in PPMS) and also heat capacity of the apiezon C_{ap}. $C_{platform}(T)$ dependences are stored in PPMS software as calibrations for different calorimeter pucks and software automatically subtracts it from C_{total} to obtain C_{sample}. $C_{ap}(T)$ dependences cannot be exactly tabulated, because we never know exact amount of Apiezon on the platform. In PPMS software we can take apiezon into account by creating puck calibration with added apiezon. More precise way is to measure only the puck with apiezon and then mount sample on the platform.

Advanced thermal model takes into account relaxation between platform and sample. This model is called *Two-tau model* in PPMS and was developed by Hwang et al. in 1997 [14]. It simulates the effect of heat flowing between the platform and the sample and vice versa. An experiment is then described with a system of two differential equations:

$$C_{platform}\ \frac{dT_p}{dt} = P(t) - K_w\left(T_p(t) - T_b\right) + K_g\left(T_s(t) - T_p(t)\right) \tag{21}$$

$$C_{sample}\ \frac{dT_s}{dt} = -K_g\left(T_s(t) - T_p(t)\right) \tag{22}$$

In comparison with the simple model, here we have additional parameters: K_g is thermal conductance between the sample and the platform (due to the Apiezon), T_s and T_p are respective temperatures of the sample and the platform. Since the temperature sensor is attached to the platform, calorimetric system records T_p value (we cannot measure $T_s(t)$ dependence). Thus we eliminate T_s and obtain only one differential equation of second order. Final solution is more complex than for the simple model but fitting to the measured data is still possible. As a result of this fit we obtain both C_{sample} and $C_{platform}$, so heat capacity of the puck is not necessary.

When measuring heat capacity on PPMS, software always computes both models and uses the one with the smallest fit deviation (chi square).

3. Previous results

3.1. CePdAl

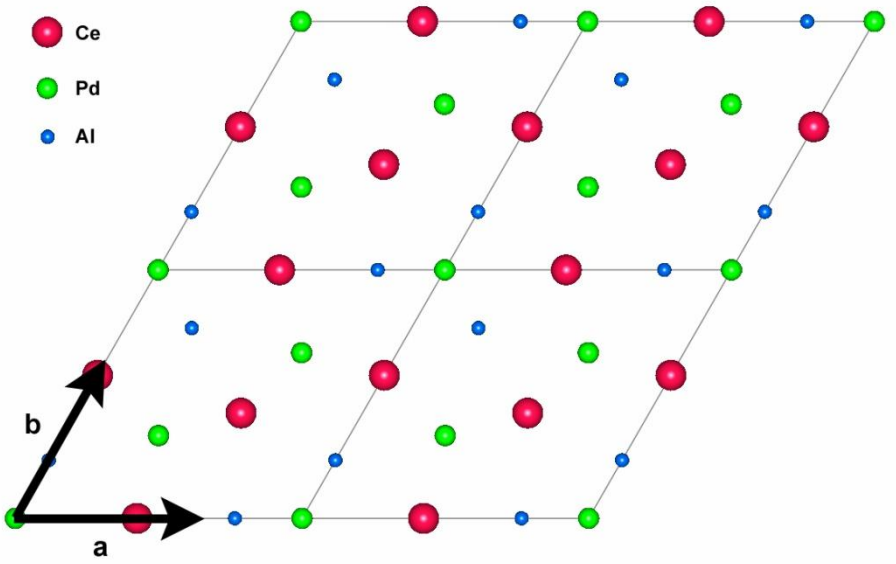

Fig. 4 - CePdAl crystal structure

CePdAl crystallizes in the hexagonal ZrNiAl-type structure (space group $P\bar{6}2m$) [15], see Fig. 4. It orders antiferromagnetically below T_N = 2.7 K [16]. The enhanced γ-value (> 200 mJ.mol^{-1}K^{-2}) indicates heavy-fermion behavior, the low value of the magnetic entropy released at T_N ($\cong 0.4\,R \ln 2$) and the temperature dependence of electric resistivity [17] give evidence for a pronounced Kondo effect. Based on the observed pressure dependence of the specific-heat anomaly [18], CePdAl seems to be located close to the maximum of T_N in Doniach's magnetic phase diagram. The long-range magnetic order below T_N = 2.7 K is characterized by an incommensurate propagation vector k = (1/2, 0, τ) with $\tau \approx 0.35$ and a coexistence of the magnetically ordered moments and disordered atoms (see Fig. 5). The ordered magnetic Ce moments are oriented along the c-axis and form ferromagnetic chains parallel to the b-axis with an antiferromagnetic coupling along the a-axis. The amplitude of the moments is constant in the a-b plane, but it varies (sine-wave modulation) along the hexagonal c-axis according to the incommensurate component τ of the propagation vector. Disordered magnetic moments on 1/3 of the Ce sites are located between ferromagnetic chains due to geometric frustration in this compound which is in a close relation to the Kagome-like triangular arrangement of Ce atoms within the basal planes [19].

The neutron diffraction reveals that the frustrated moments do not order down to 180 mK at least [20]. The single-crystal magnetization measurements [21] reveal a strong magnetocrystalline anisotropy with the c-axis as the easy axis, in agreement with the diffraction data. Recently, the dilution effects in $Ce_{1-x}Y_xPdAl$ [22] and $Ce_{1-x}La_xPdAl$ [23] have been studied. The substitution of Ce ions by nonmagnetic ions leads to a gradual suppression of magnetic order, the reduction of T_N being stronger for the Y substitution. The long-range magnetic order disappears also when Pd is substituted by Ni or Rh [24].

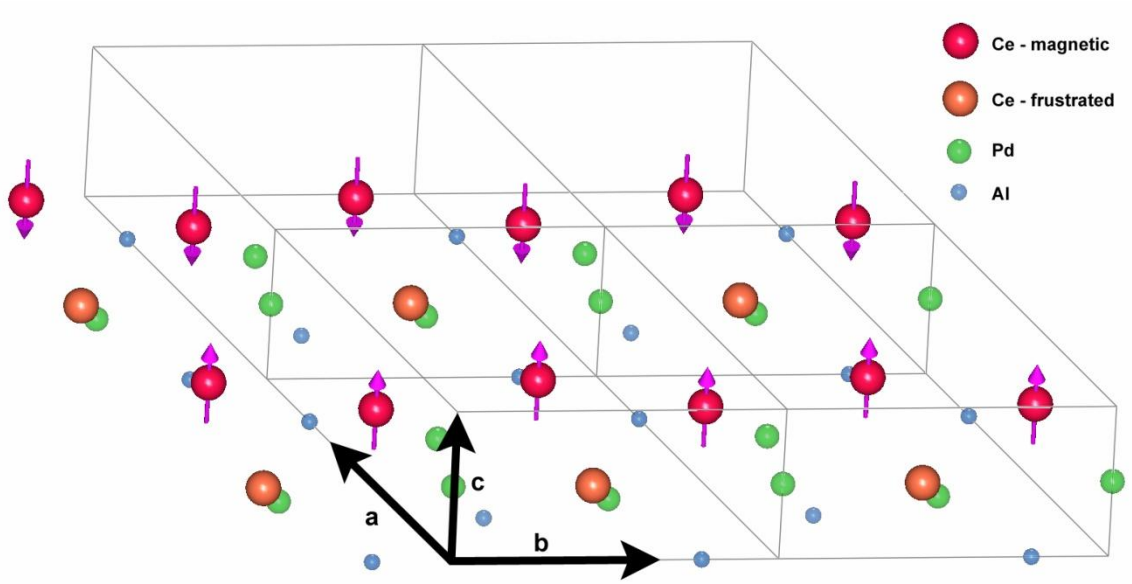

Fig. 5 – CePdAl magnetic structure

3.2. Ce(Cu,Al)$_4$

The Ce-Cu and the Ce-Al binary systems contain many heavy-fermion compounds, deeply studied in the past. Thus it is expected that also Ce-Cu-Al ternary systems contains interesting materials, especially in the cerium corner. Systematic study of these compounds provided Raghavan [25] and recently also Hu et al. [26]. We are interested in area marked B in Fig. 6 - compounds with $CeCu_xAl_{4-x}$ ($0.7 \leq x \leq 1.1$) stoichiometry. They crystallize in the tetragonal $BaAl_4$-type structure (space group I4/mmm) [26], but for special case where $x = 1$ ($CeCuAl_3$), the $BaNiSn_3$-type structure (space group I4mm) is reported. These structures are very similar, because $BaNiSn_3$ is a special case of $BaAl_4$ with lower symmetry – see Fig. 7.

$CeCuAl_3$ has been reported to order antiferromagnetically below $T_N \sim 2.5 - 2.9$ K [27]. The interplay between the magnetic and Kondo interactions has been used to describe the observed specific-heat, magnetic-susceptibility [28], electrical-resistivity [29] and NMR data [30]. A relatively small crystal-field (CF) splitting of 10 and 180 K between the ground state and the first and second excited doublet, respectively, has been deduced from the magnetization measurements on a single crystal [29].

The magnetization and the zero-field specific heat of $CeCu_xAl_{4-x}$ compounds with x = 0.8, 0.9, 1.0 and 1.1, measured on single crystals, reveal the a-axis as the easy magnetization axis and a clear strengthening of the ferromagnetic interactions with decreasing Cu content [31]. The ordering temperature shows only weak concentration dependence and the crystal-field splitting deduced from the magnetization curves increases roughly linearly with decreasing x.

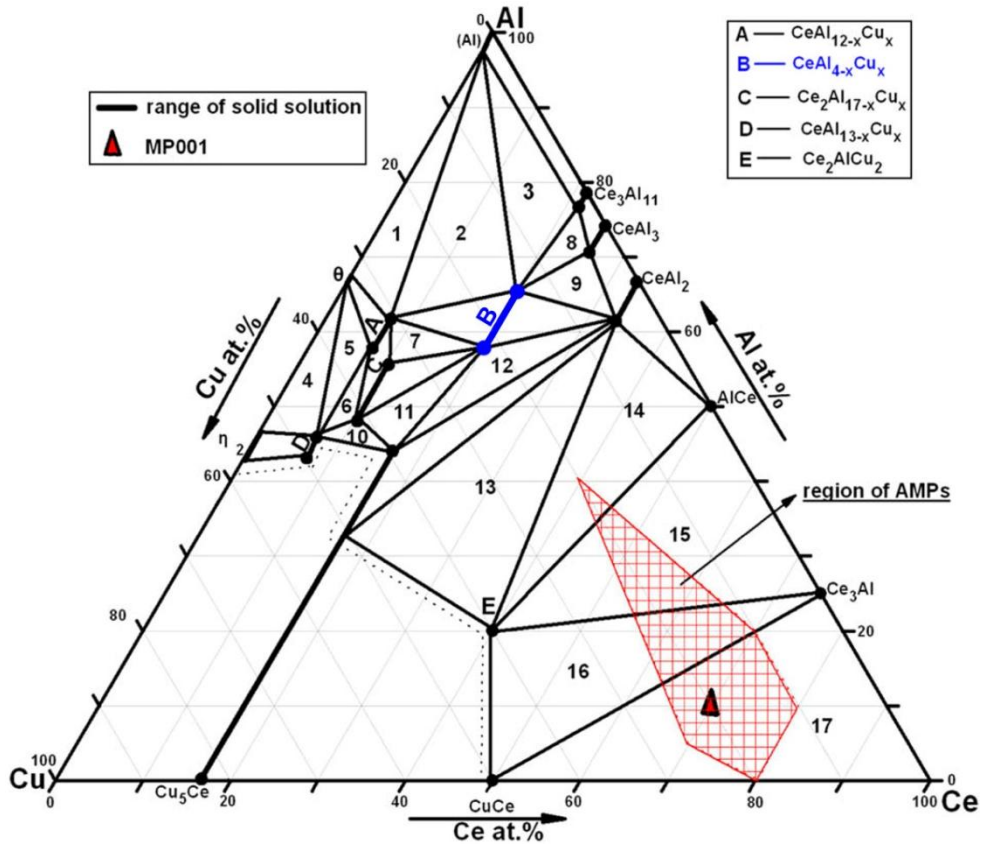

Fig. 6 - The phase composition of as-cast alloys formed by conventional arc-melting in the ternary Ce–Al–Cu system with Cu content less than about 50 at.% (take from [26]).

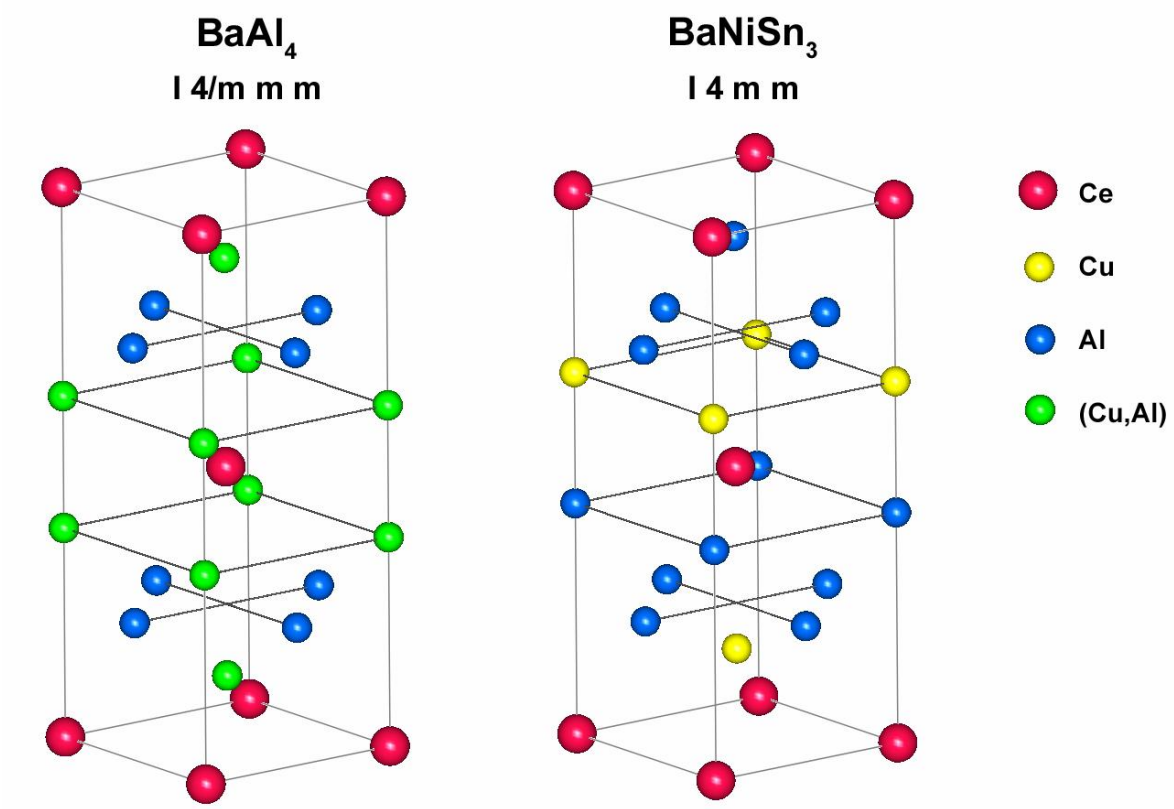

Fig. 7 – Comparison of $BaAl_4$ and $BaNiSn_3$-type structures for $Ce(Cu,Al)_4$ series.

3.3. Ce(Ni,Cu)Al series

Both CeNiAl and CeCuAl compounds crystallize in the hexagonal ZrNiAl-type structure (space group P-62m; refer Chapter 3.1 and Fig. 4). Previous studies on CeNiAl showed attributes of a non-magnetic mixed-valence system with low γ-value of the electronic specific heat. The magnetic susceptibility does not show Curie-Weiss behavior; instead, it weakly increases with increasing temperature up to 350 K and shows no indication of magnetic ordering down to 2 K [32]. On the other hand, CeCuAl has clear trivalent state Ce^{3+}, orders magnetically at temperatures below 5 K and the specific heat indicated enhanced γ-value [32]. Synthesis of the CeCuAl compound is not easy, while it does not melt congruently. An annealing treatment enhances sample quality, but never eliminates all impurities phases [33].

Ce(Ni,Cu)Al series could illustrate transition from the mixed-valent state of CeNiAl to the trivalent state in CeCuAl. Disappearance of the mixed-valent behavior with increasing copper concentration is expected.

4. Experimental, results and discussion

I decided to unconventionally connect these three parts together due to preservation of continuance in a study of individual compounds.

4.1. (Ce,Y)PdAl

Polycrystalline samples of $Ce_{1-x}Y_xPdAl$ with x = (0; 0.02; 0.04; 0.06; 0.08; 0.1; 0.15; 0.2; 0.3; 0.5; 0.8) were prepared by arc-melting stoichiometric mixtures of pure elements (4N for Ce and Y, 3N5 for Pd and 5N for Al) in mono-arc furnace. Samples were melted under protection of argon atmosphere, turned and re-melted several times to achieve better homogeneity. Phase analysis was done on X-ray powder difractometer Bruker D8 Advance using Bragg-Brentano geometry. Analysis of the diffraction pattern was done using standard Rietveld method in the Fullprof software [34].

The experiments on the powdered as-cast samples at room temperature showed all to be single phase with the hexagonal ZrNiAl-type structure. Since an annealing process causes a chemical decomposition, as-cast samples were used in this study.

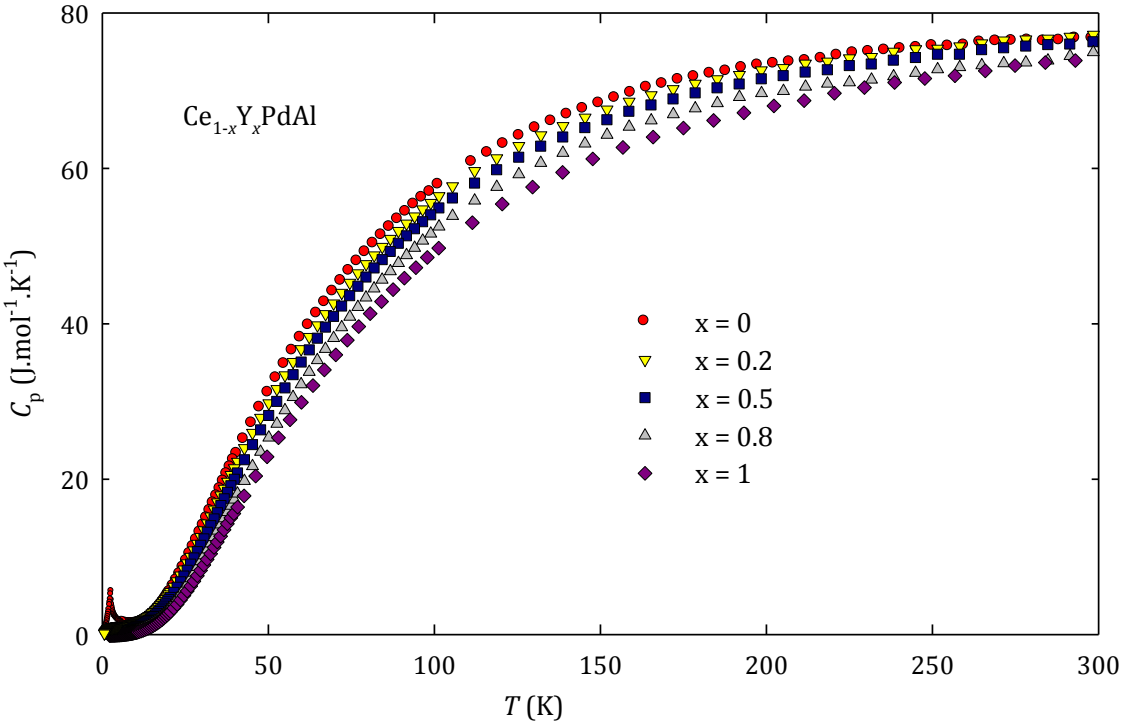

Fig. 8 - The specific heat of the $Ce_{1-x}Y_xPdAl$ compounds in the whole measured temperature range. Only selected representative concentrations are shown.

The specific heat was measured on PPMS system in the temperature range between 0.35 and 300 K and in magnetic field up to 14 T. Small samples with the mass of about 2 mg were used for measurement at low temperatures below 10 K and in magnetic fields, whereas larger samples (~ 20 mg) were used for measurements between 2 and 300 K to achieve reasonable precision at higher temperatures, where the heat capacity of the sample holder increases considerably.

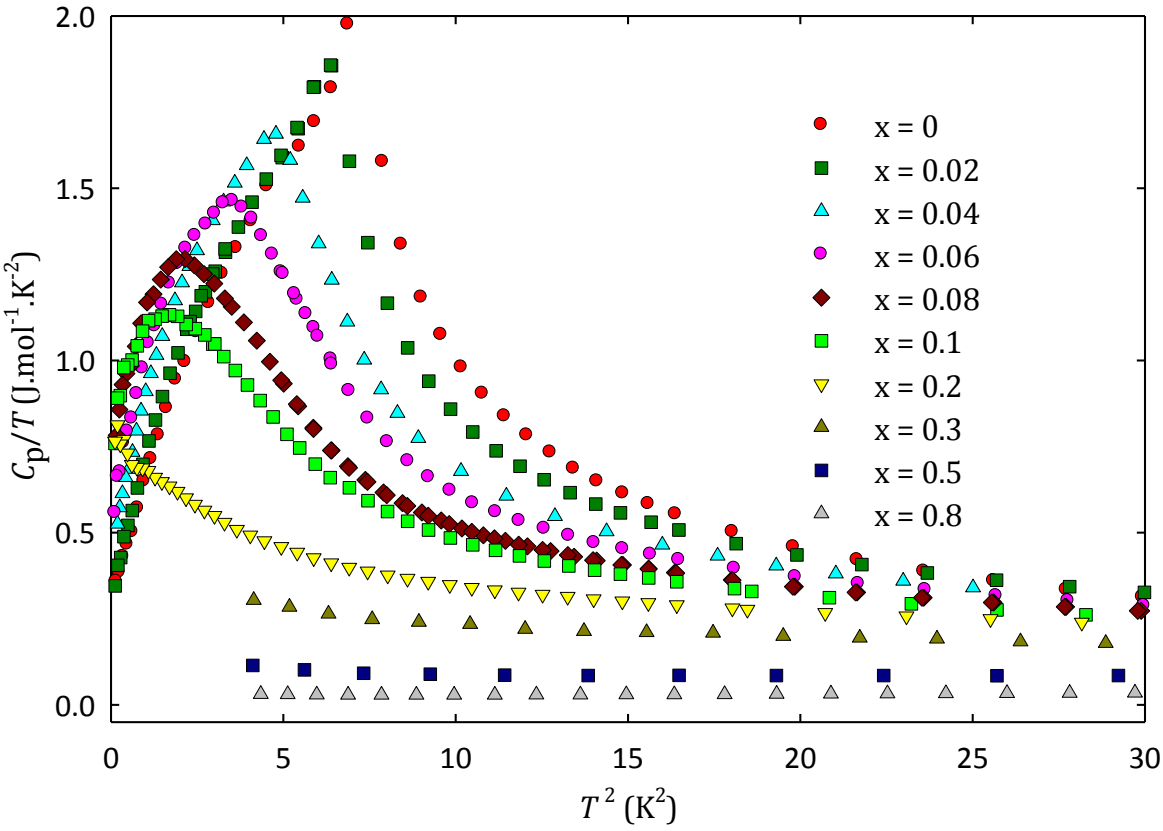

Fig. 9 - Low-temperature specific heat of the $Ce_{1-x}Y_xPdAl$ compounds.

4.1.1. Overall specific heat

The specific heat of the $Ce_{1-x}Y_xPdAl$ compounds is represented in Fig. 8 and the low-temperature detail in Fig. 9. Measured specific heat of pure CePdAl is in accordance with data presented in [17] and [16]. We observe a well pronounced anomaly with a maximum at 2.7 K. The shape of this anomaly is typical for a second-order phase transition. The idealization of the specific-heat jump under the constraint of entropy conservation yields the ordering temperature T_N = (2.8 ± 0.1) K, in agreement with previous experiments. The anomaly shifts to lower temperatures with increasing the Y content and the corresponding concentration dependence of T_N is plotted in Fig. 10. The accuracy of the T_N determination decreases with Y content as the anomaly becomes broader. The magnetic order vanishes for compounds with ≃ 20% of Y.

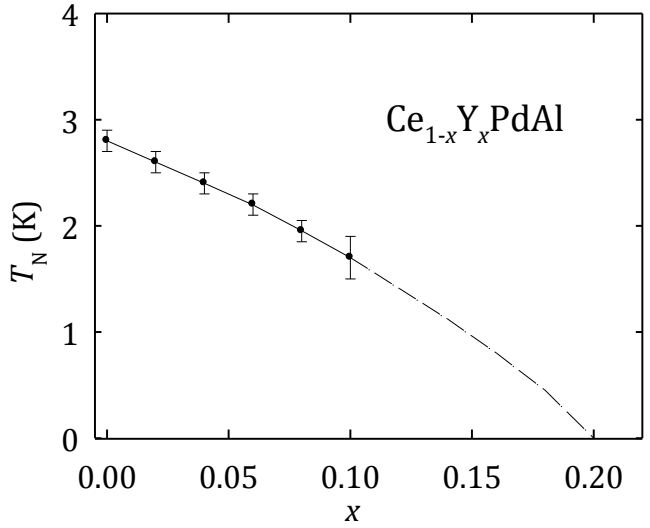

Fig. 10 – The concentration dependence of the Néel temperature; the dashed line here is an extrapolation only.

The measured $Ce_{0.8}Y_{0.2}PdAl$ data show still a relatively strong increase of C_p/T with decreasing temperature which is qualitatively similar to the rise of specific heat observed for $T > T_N$ in compounds with lower Y concentration. We cannot thus exclude that

$Ce_{0.8}Y_{0.2}PdAl$ orders magnetically with T_N below 0.4 K. On the other hand, such upturn of C_p/T at low temperatures is often observed in diluted systems for compounds on the edge of the long-range magnetism [35]. Similar behavior was observed also for compounds from the Ce(Pd,Rh)Al series that do not show the long-range magnetic order. The low-temperature data were described there by a power-law behavior $C_p/T \sim T^{-n}$ with n between 0.2 and 1.2 depending on the Pd-Rh concentration [36]. The $Ce_{0.8}Y_{0.2}PdAl$ data below $\approx$ 6 K can be also well described by such a power-law with n around 0.5.

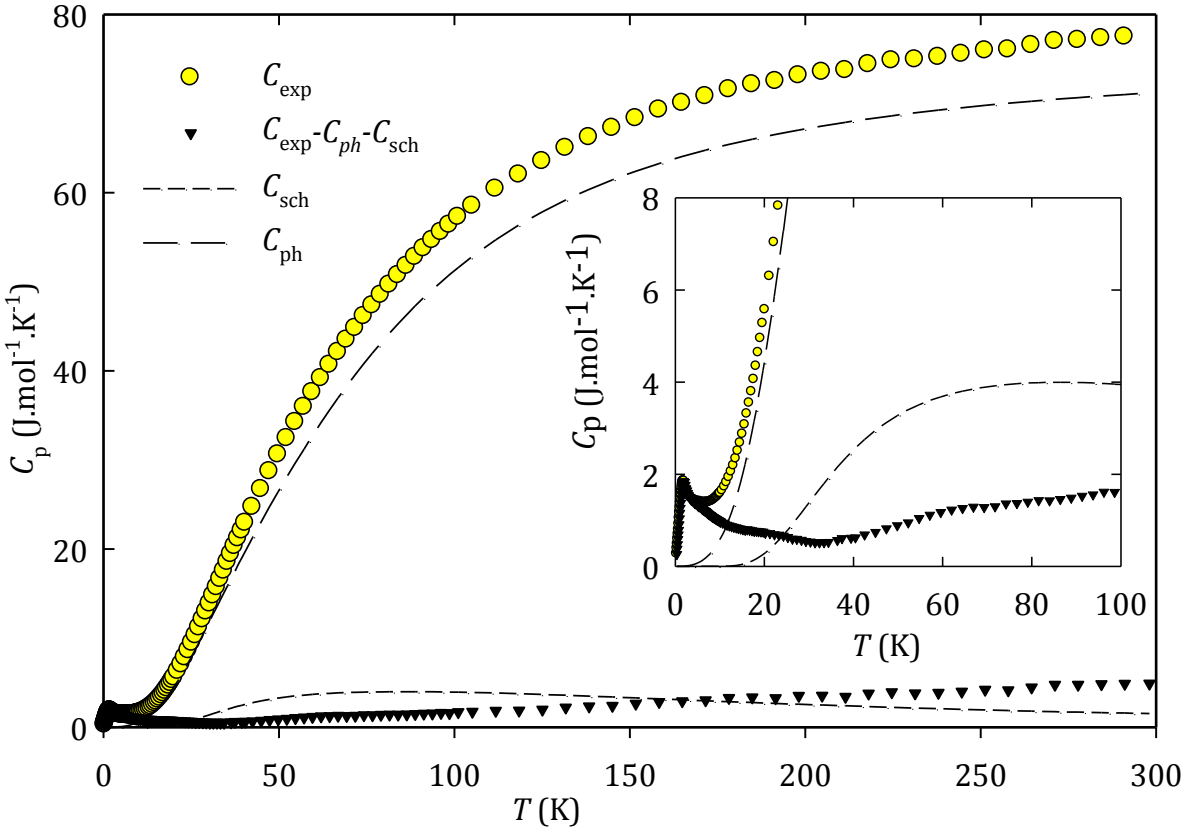

Fig. 11 - All contributions to the specific heat for $Ce_{0.9}Y_{0.1}PdAl$. The lattice contribution was calculated using θ_D = 150 K, θ_{E1} = 159 K and θ_{E2} = 311 K. The Schottky contribution was obtained using Δ_1 = 169 K and Δ_2 = 409 K [37].

A very detailed analysis of high temperature specific heat contributions in the whole (Ce,Y)PdAl series was described in my bachelor thesis [37]. I will present here only brief overview and the results, to keep reader in a context.

Certain quantitative estimation can be easily done for the γ value at 300 K, which is crucial point in the analysis. The lattice contribution is rather flat at temperatures close to 300 K and we can assume similar values for all Y concentrations. This assumption is corroborated by the fact that the specific heat of YPdAl and LuPdAl show only a small difference at 300 K [38]. The Schottky contribution can be also considered small and only weakly concentration dependent at 300 K. The difference between the measured specific heat of CePdAl and YPdAl (γ_{YPdAl} = 5.9 mJmol^{-1}K^{-2} [38]) at 300 K (see Fig. 8) is thus predominantly due to the electronic specific heat. The measured values indicate that the γ coefficient at 300 K is 15 $\pm$ 5 mJ.mol^{-1}K^{-2} for CePdAl and the Ce rich compounds. This value is much lower than the enhanced low-temperature γ value (> 200 mJmol^{-1}K^{-2}) reported previously [17] and

observed also in our data. It follows that there should be a strong increase of the electronic specific heat with decreasing temperature. This qualitative conclusion is quite indisputable considering also definite uncertainty in the lattice or Schottky contributions. The temperature dependence of C_{el}/T at low temperatures is observed frequently in heavy-fermion systems [39] and also in systems with moderately enhanced γ coefficient including e.g. δ-Pu [40].

Exact analysis (see Fig. 11 for example of all contributions for chosen concentration $x = 0.1$) confirms our qualitative conclusion. Temperature dependence of the electronic specific heat is shown in Fig. 12.

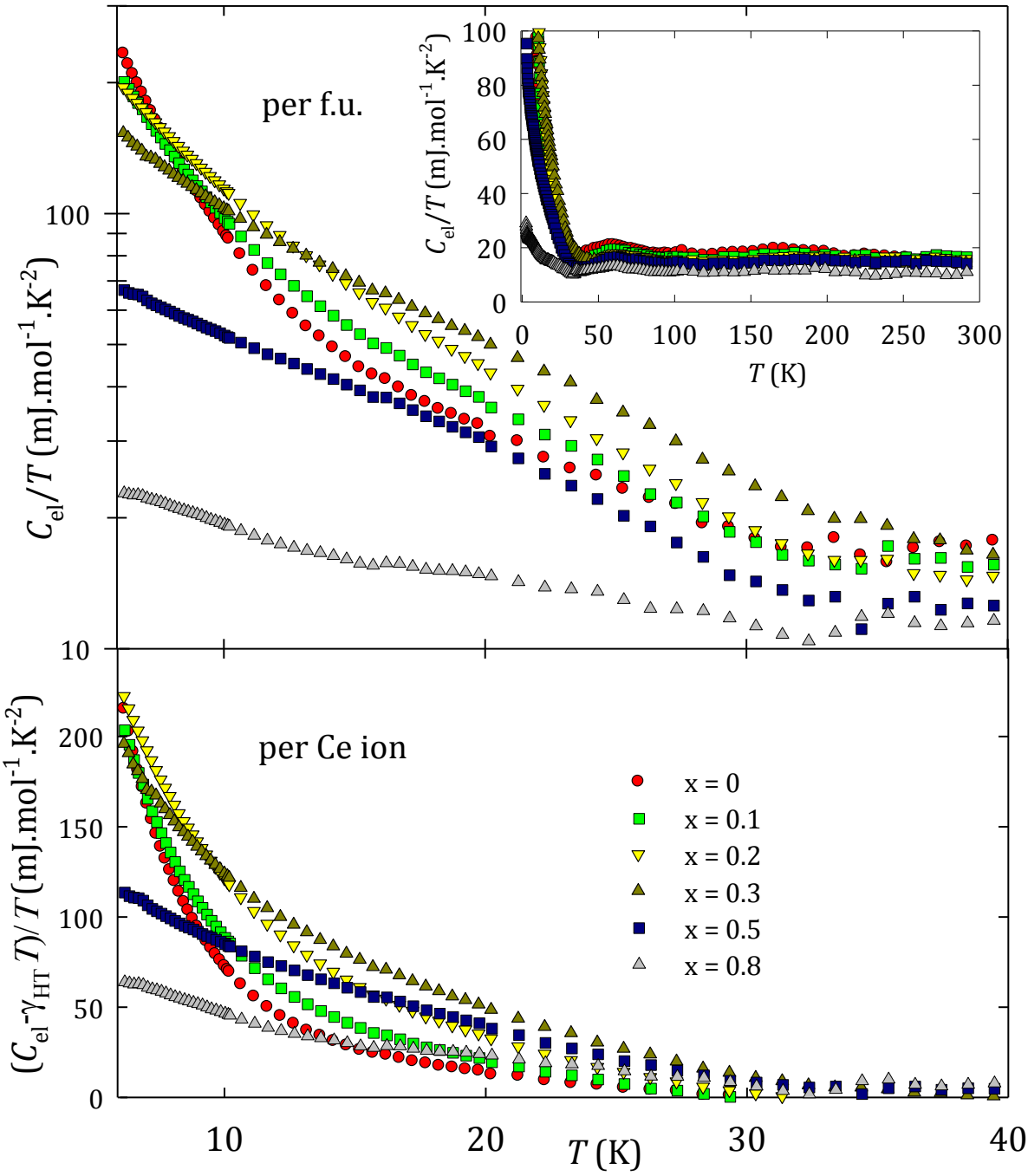

Fig. 12 - The temperature dependence of the electronic specific heat. The values per (Ce,Y)PdAl formula unit are presented in the top plot (note the logarithmic scale), in the inset is shown the same dependence in whole temperature range. The values of enhanced γ per Ce ion are presented in the bottom plot (standard scale).

4.1.2. Low temperature magnetic specific heat

Let us now describe the specific heat of CePdAl in the magnetically ordered state. The lattice contribution is very small below 5 K. We can easily use the lattice specific heat of isostructural LuPdAl as an approximation for CePdAl without introducing any noticeable error. The remaining sum of the electronic and magnetic specific heat well below T_N is described by the following expression in accordance with (11) and (18):

$$C_{el} + C_M = \gamma T + A_{mag}\, T^{\frac{d}{m}} \exp\frac{-\delta}{T} \tag{23}$$

The A_{mag} coefficient is related to the spin velocity in the magnetically ordered state [41]. Measured low temperature $C(T)$ dependence can be described without the exponential term, which means that there could be no gap in a magnon dispersion curve of CePdAl.

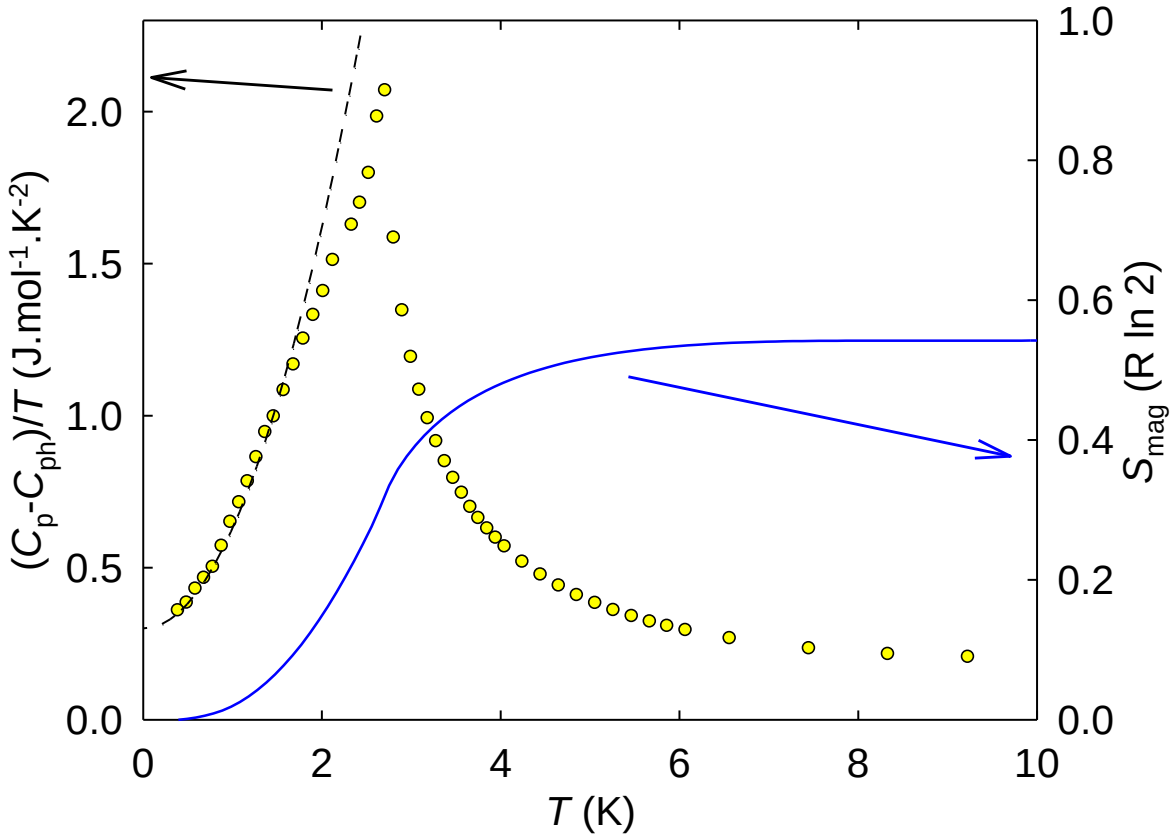

Fig. 13 - The specific heat and magnetic entropy of CePdAl. The dashed line represents the fit to equation (23) below 1.8 K (see text for details).

The limited temperature region which can be described by expression (23) does not allow for plausible determination of the parameter d/m. Assuming 3-dimensional antiferromagnetic order, the CePdAl data can be satisfactory described by equation (23) below 1.8 K (see Fig. 13). The fit of experimental data gives $\gamma = 300 \pm 30$ mJ.mol^{-1}K^{-2}, slightly higher than the value of 250 mJ.mol^{-1}K^{-2} deduced from previous specific-heat measurements [17]. Taking values of d/m between 3 and 2, corresponding to lower dimensionality of the antiferromagnetic order as discussed also in [42], we obtain the γ-values between 250 and 300 mJ.mol^{-1}K^{-2}. Similar result is achieved for $Ce_{0.98}Y_{0.02}PdAl$, the analysis for higher Y concentrations is less reliable due to decreasing of T_N.

Taking $\gamma = 300$ mJ.mol^{-1}K^{-2} as the low-temperature limit, $\gamma = 200$ mJ.mol^{-1}K^{-2} at 10 K and a linear interpolation between these values, we can subtract electronic specific heat from total measured data to obtain C_M. It is then possible to calculate the molar magnetic entropy at T_N as 0.35 $R \ln 2$, see Fig. 13. This value is in accordance with reference [16], but smaller than the value of 0.55 $R \ln 2$ given in [17] by Schank et al. Taking into account very good agreement between our data and data determined by Schank, we guess that the entropy value in [17] might correspond to both C_M and C_{el} which are difficult to separate. This approach with our data would lead to the entropy value at T_N of 0.51 $R \ln 2$ in accordance with Schank. The magnetic entropy continues to increase in a relatively broad temperature range above T_N up to ~ 6 K, indicating strong magnetic fluctuations even far above T_N. This result is consistent with the temperature dependence of the nuclear magnetic relaxation rate as observed in a recent ^{27}Al NMR measurements [42]. The value of magnetic entropy at 10 K amounts 0.54 $R \ln 2$, considerably below the value expected for a doublet ground state. The strong reduction of the magnetic entropy can be ascribed to a Kondo effect.

4.1.3. Kondo effect evaluation

We have estimated T_K considering the reduction of the magnetic entropy at T_N with respect to the value of Rln2 using equation (19). The results depend on the way how we calculate the magnetic entropy S_0. It can be estimated from $C_M + C_{el}$ as in [7], or only from C_M. Calculating the entropy per Ce mol from $C_M + C_{el}$ leads to Kondo temperatures between 5 - 6 K. With increasing Y concentration T_K slightly decreases as can be seen from Fig. 14. Calculating T_K only from C_M we get somewhat higher Kondo temperatures values (7 K for CePdAl) with the same concentration trend.

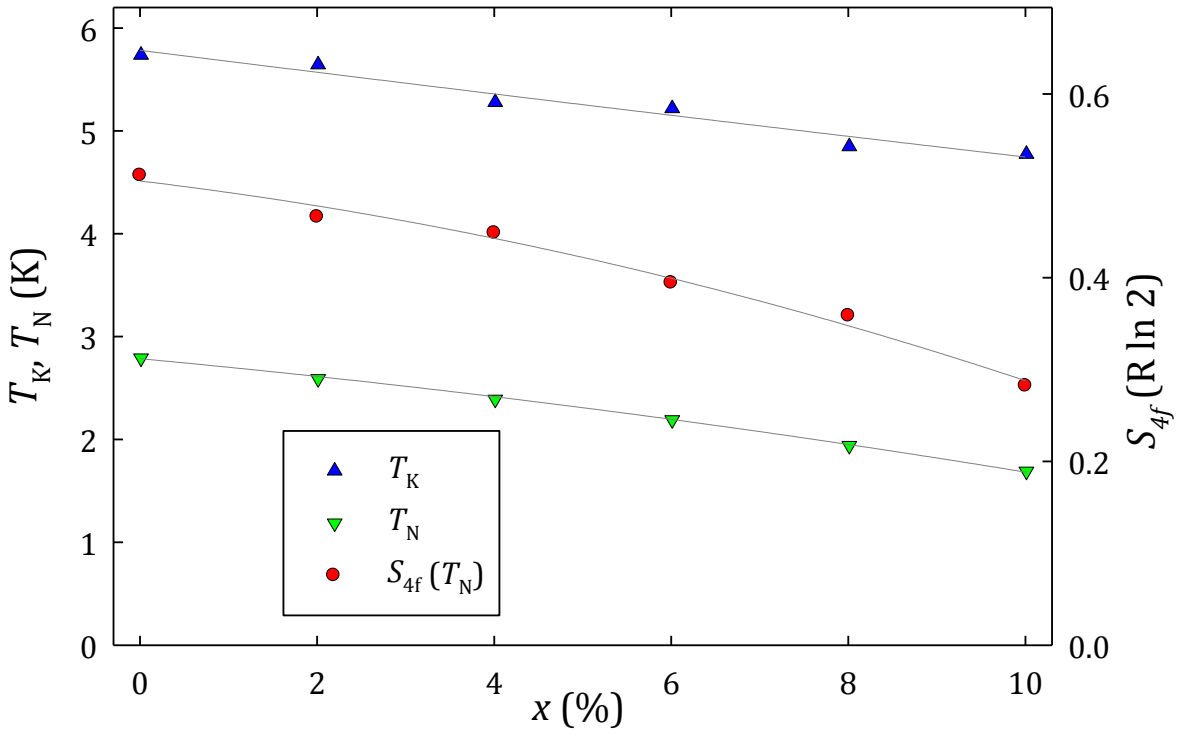

Fig. 14 - Dependence of the Kondo temperature and the 4f-electron entropy (per Ce mol) at T_N on Yttrium concentration. We present also the Néel temperature shown already in Fig. 10 to allow direct comparison. Dotted lines are only to guide an eye with no physical meaning.

4.1.4. Specific heat in external magnetic field

The influence of applied magnetic field on the specific heat is presented in Fig. 14 for pure CePdAl. Here we should have in mind that CePdAl is a strongly anisotropic system and we present measurements on polycrystalline samples. The observed effect represents thus only an average over all field directions with respect to the crystal structure. The magnetization [43] and neutron diffraction [44] single-crystal measurements reveal several metamagnetic transitions between 3 and 4 T for field applied along the c-axis. Although the exact origin of these metamagnetic transitions remains unknown, it was speculated that they are connected with the onset of magnetic moment appearance on the frustrated 1/3 of the Ce

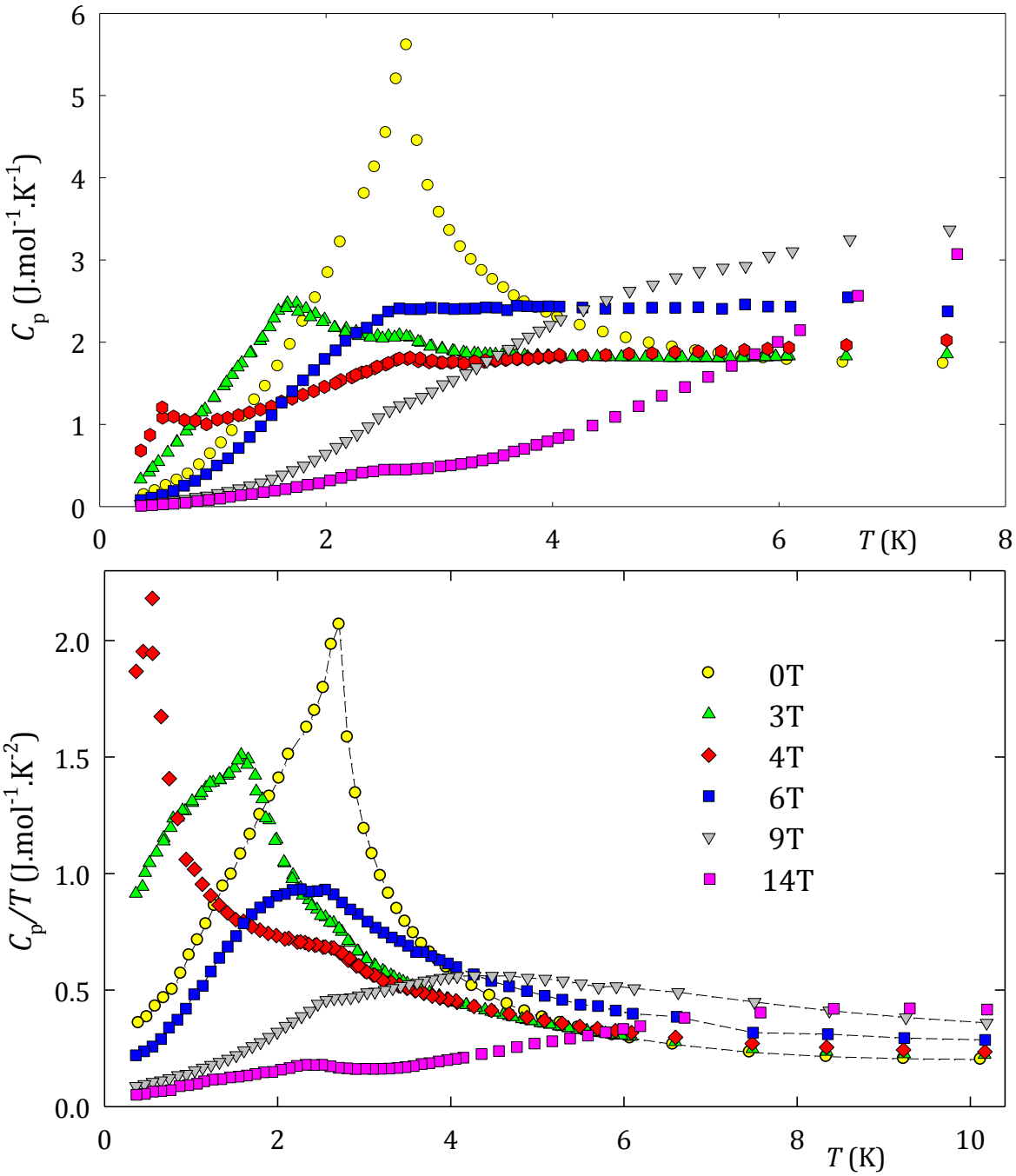

Fig. 15 - The specific heat of the CePdAl compound measured in external magnetic fields displayed as C_p vs T and $\frac{C_p}{T}$ vs T plots. The legend presented in second plot holds for both.

sites and subsequent appearance of a ferromagnetic component on the remaining Ce sites. On the other hand, the magnetic field applied perpendicular to the c-axis does not break the antiferromagnetic order and corresponding magnetization curve shows no transitions up to 7.5 T [21]. Our data for pure CePdAl (see Fig. 15) are generally in agreement with these observations. The anomaly around T_N first shifts gradually to lower temperatures as expected for the antiferromagnetic order. The specific heat above 3 K remains almost unchanged in fields up to 4 T. Further increase of the magnetic field above 4 T leads to a considerable increase of C_p/T at temperatures above 3 K. The magnetic entropy is thus shifted to higher temperatures indicating ferromagnetic ordering in CePdAl above 4 T, in agreement with the magnetization and neutron diffraction data. The unchanged antiferromagnetic order for grains oriented perpendicular to the magnetic field is reflected by persisting anomaly around $T_N = 2.7$ K. This anomaly is clearly observed even in the field of 14 T. Another observation concerns the low-temperature limit of the electronic specific heat which is reduced in magnetic fields above 4 T, leading to $\gamma \simeq 50$ mJ.mol^{-1}K^{-2} in 14 T. The decrease of the γ-value in the field-induced ferromagnetic state, where the frustration of 1/3 of Ce moments is lifted [34], corroborates the suggestion that the one third of the Ce moments that are frustrated (paramagnetic) are in a heavy-fermion state [42].

The compound with 2 % yttrium shows behavior similar to CePdAl. With further increasing the yttrium content between 4 and 8 %, the anomaly around T_N becomes broader in zero field. The application of magnetic field leads to shift of the anomaly to lower temperatures as for pure CePdAl, but the anomaly that persisted at 2.7 K disappears for yttrium concentration above 6 %. From specific heat data we can only speculate that the absence of this latter anomaly is an indication of reducing the strong magnetocrystalline anisotropy in CePdAl. Measurement of specific heat in the external magnetic field for the samples with yttrium was done mainly by Mr. Prchal, so appropriate plots are not part of this thesis. Please refer to [45] where the results are published.

4.1.5. Powder neutron diffraction

We have performed neutron diffraction experiment in Helmholtz Zentrum Berlin (HZB). The goal of the experiment is to investigate the effect of Y substitution on the magnetic structure of CePdAl. We would clarify if there appears any magnetic moment on the frustrated Ce sites and if there will be any propagation vector change with Y substitution.

Samples of $Ce_{1-x}Y_xPdAl$ with x = (0.02; 0.06; 0.1; 0.15) were additionally prepared with the same technique as previous one. These samples are also tested with X-ray diffraction for the phase purity. Powder neutron diffraction was investigated at HZB on the multicounter powder neutron focusing diffractometer E6. It is equipped with a horizontally and vertically bent monochromator consisting of 105 pyrolytic graphite crystals mounted on a matrix leading to a relatively high flux (5.10^6 n/cm^{2}s) at the sample position [46]. There are two position sensitive multi-detectors with oscillating radial collimator for background reduction. The incident neutron wavelength of $\lambda = 2.438$ Å was determined in advance using a YIG sample.

Measured data were first analyzed with the BEAN software build on PV-Wave framework. This program can summarize data from both multidetectors and integrate

obtained 2D map along Debye-Sherrer cone to obtain only intensity vs. 2θ dependence. Crystal and magnetic structures were then simultaneously refined by the Fullprof program.

Samples with x = 0.02 and 0.06 were measured in orange cryostat at two temperatures: 1.3 K for magnetically ordered region and 8 K for paramagnetic state. Lower ordering temperature is expected for the sample with x = 0.1 and temperature 1.3 K (the limit for orange cryostat) will not be low enough (see Fig. 10). So this sample was measured in He3-He4 dilution refrigerator at temperatures: 0.4 K, 1.3 K (for comparison) and 8 K.

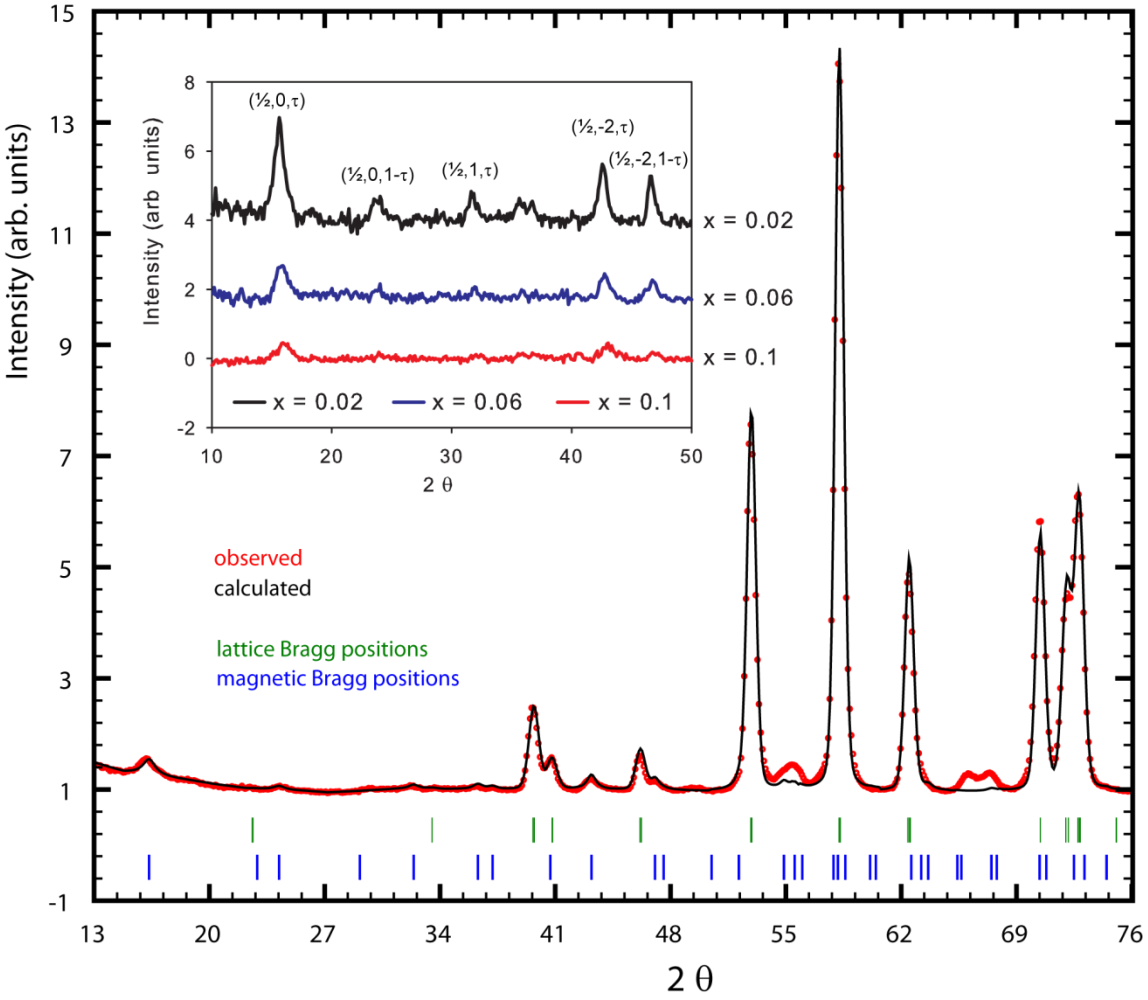

Fig. 16 - FullProf refinement of the crystal and magnetic structures of CePdAl at 1.3 K. The inset shows differences between paramagnetic and ordered diffraction patterns for all measured $Ce_{1-x}Y_xPdAl$ compounds.

Diffraction pattern analysis at 8 K confirms purity of the powdered samples. Diffraction patterns recorded at 1.3 K contain additional Bragg reflections arising from scattering on the ordered magnetic moments of Ce atoms. We have determined from the positions of these magnetic peaks, that the propagation vector keeps unchanged for all measured concentrations and is in agreement with a measurement done by Dönni at al. on the pure CePdAl [19]. Standard overall magnetic structure refinement was rather difficult, because magnetic reflections are very weak – especially in the sample with $x = 0.1$. Therefore we decided to reveal changes in magnetic structure following intensities of the two strongest magnetic peaks (½, 0, τ) and (½, -2, τ) – see inset of the Fig. 16. Comparing ratio of the area of two largest

magnetic peaks in each pattern will reveal changes in magnetic structure. They do not change significantly so only changing parameter along the series is only height of the magnetic peaks.

However if we remove frustration on ⅓ of Ce atoms, ratio of the area of the examined peaks does not change radically and possible removing of the frustration with increasing yttrium concentration cannot be negated.

Exact refinement of $Ce_{0.98}Y_{0.02}PdAl$ from Fullprof program is presented in Fig. 16. Reflections on $2\theta = 55°$ and around $2\theta = 66°$ are caused by sample can and does not influence purity of the sample. Determined magnetic structure parameters were propagation vector $k = (0.5, 0, \tau)$, with $\tau = 0.357(2)$, and magnitude of the ordered magnetic moments $\mu_1 = 1.62(5)\mu_B$. These values are in exact agreement with the values from [19]. See Fig. 5 for detailed magnetic structure.

4.2. CeCuAl3

Single crystals of $CeCu_{0.7}Al_{3.3}$ were prepared by the solution growth method from an aluminum flux with two different starting compositions $Ce_1Cu_3Al_{16}$ and $Ce_1Cu_2Al_{15}$, the latter one being the same as used in [47]. The elements were put into alumina crucibles, sealed under high vacuum and heated up to 1200 °C. Then, the samples were slowly cooled down to 700 °C where the remaining copper-aluminum solution was centrifuged. In this way, rather large single crystals with a size about 4x4x2mm^3 were obtained (Fig. 17).

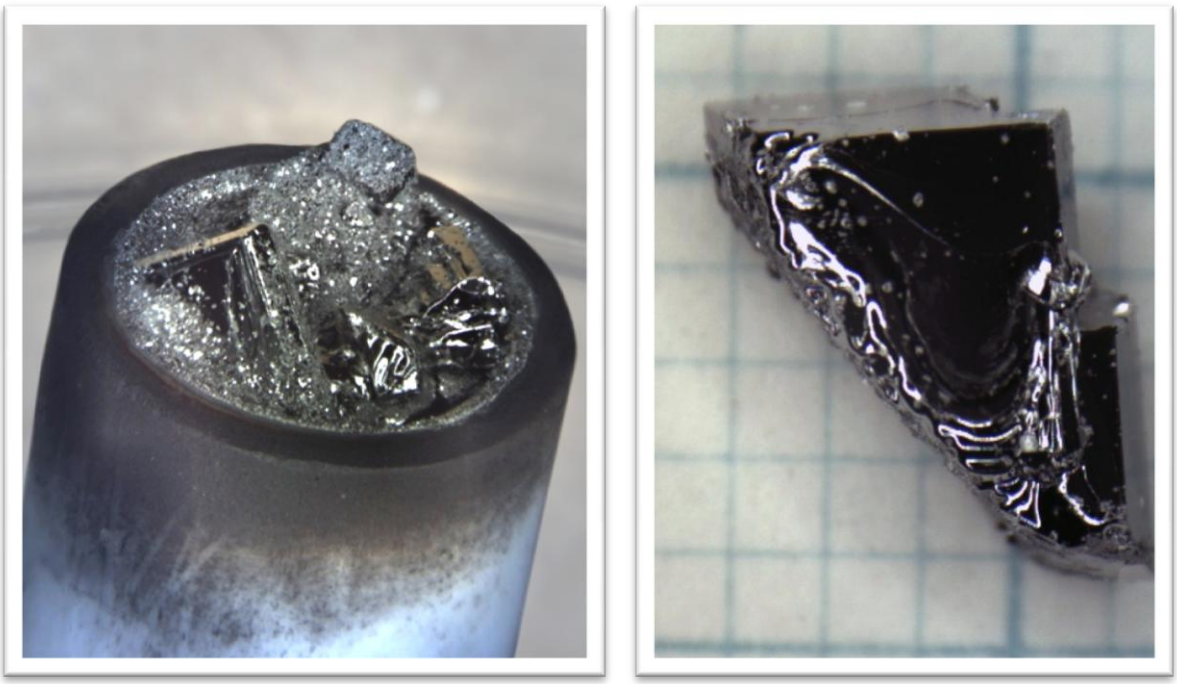

Fig. 17 – On the left picture is a photo of the alumina crucible with grown crystals. On the right side is a detail of the grown crystal of $CeCu_{0.7}Al_{3.3}$.

The sample composition and homogeneity were checked by X-ray powder diffraction (XRPD) and a scanning electron microscope (SEM) Tescan Mira I LMH equipped with an energy-dispersive X-ray detector (EDX) Bruker AXS (non-standard method). A high voltage of 10 kV was used for the analysis.

XRPD analysis has confirmed the tetragonal $BaAl_4$-type structure of the prepared sample with the lattice parameters $a = 4.262$ Å and $c = 10.776$ Å. Our idea was to determine exact composition along the blue B line in Fig. 6 from EDX microprobe analysis. Although EDX analysis confirmed a homogenous Cu-Al distribution (Fig. 18), quantitative analysis of the composition has a rather large experimental error due to the partial overlap of Ce M-α and Cu L-α spectral lines. Therefore, we have determined the actual composition by comparing the lattice parameters obtained from XRPD with those of polycrystalline $CeCu_xAl_{4-x}$ samples, as done also by Oe et al. [47]. This comparison points to composition with $x \cong 0.7$, the same as reported by Oe.

The composition was found to be similar for all crystals from both batches ($Ce_1Cu_3Al_{16}$ and $CeCu_2Al_{15}$). This can be explained from ternary diagram on Fig. 6, because composition with $x = 0.7$ is a boundary point of homogeneous phase. A crystal grown from the 1:3:16 starting composition was used for specific heat measurements.

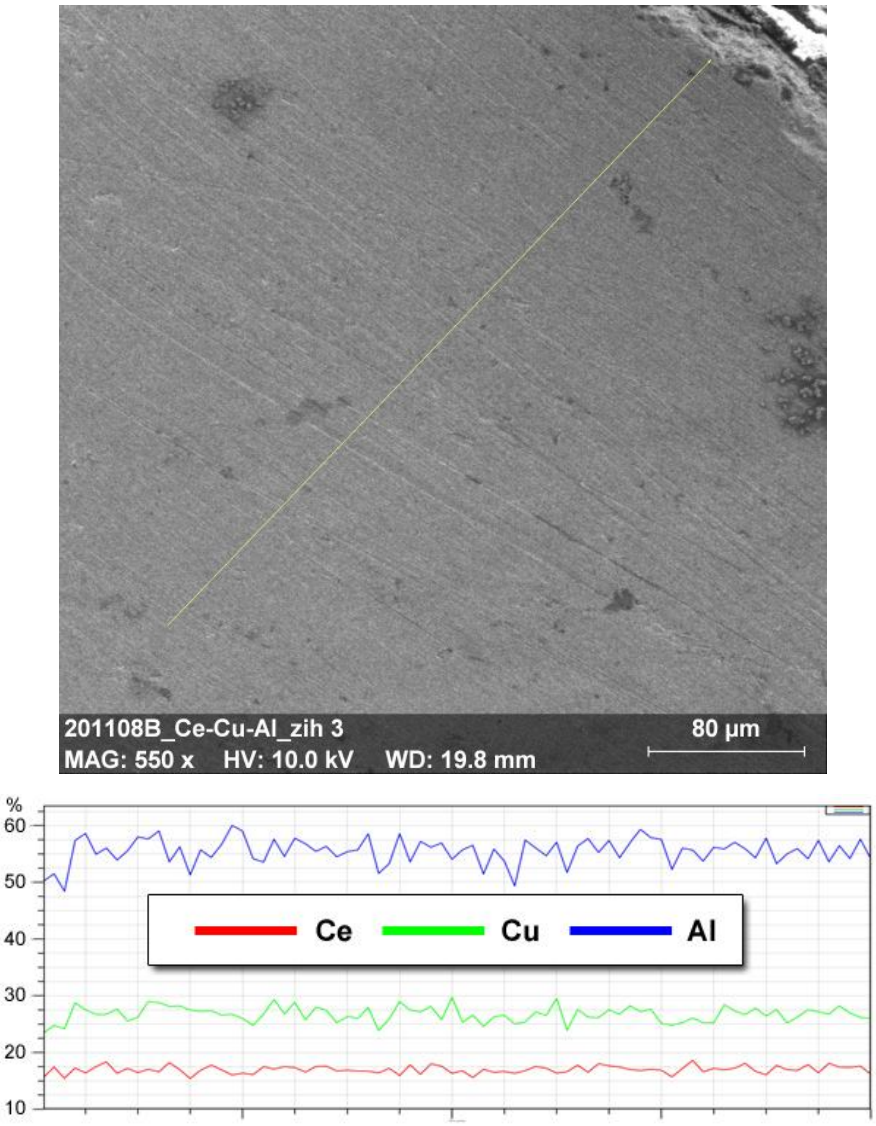

Fig. 18 – EDX line scan confirms homogeneity in the whole crystal. In the graph are shown percents of atomic weight along the line.

4.2.1. Specific heat measurements

The specific heat was measured using a Quantum Design PPMS system in the temperature range between 0.35 and 300 K and in magnetic fields up to 3 T applied along the a-axis. Small samples with a mass of about 2 mg were measured at temperatures below 10 K and in magnetic fields whereas, in order to archive reasonable precision at higher temperatures where the heat capacity of the sample holder increases considerably, larger samples (~ 20 mg) were used for measurements between 2 and 300 K.

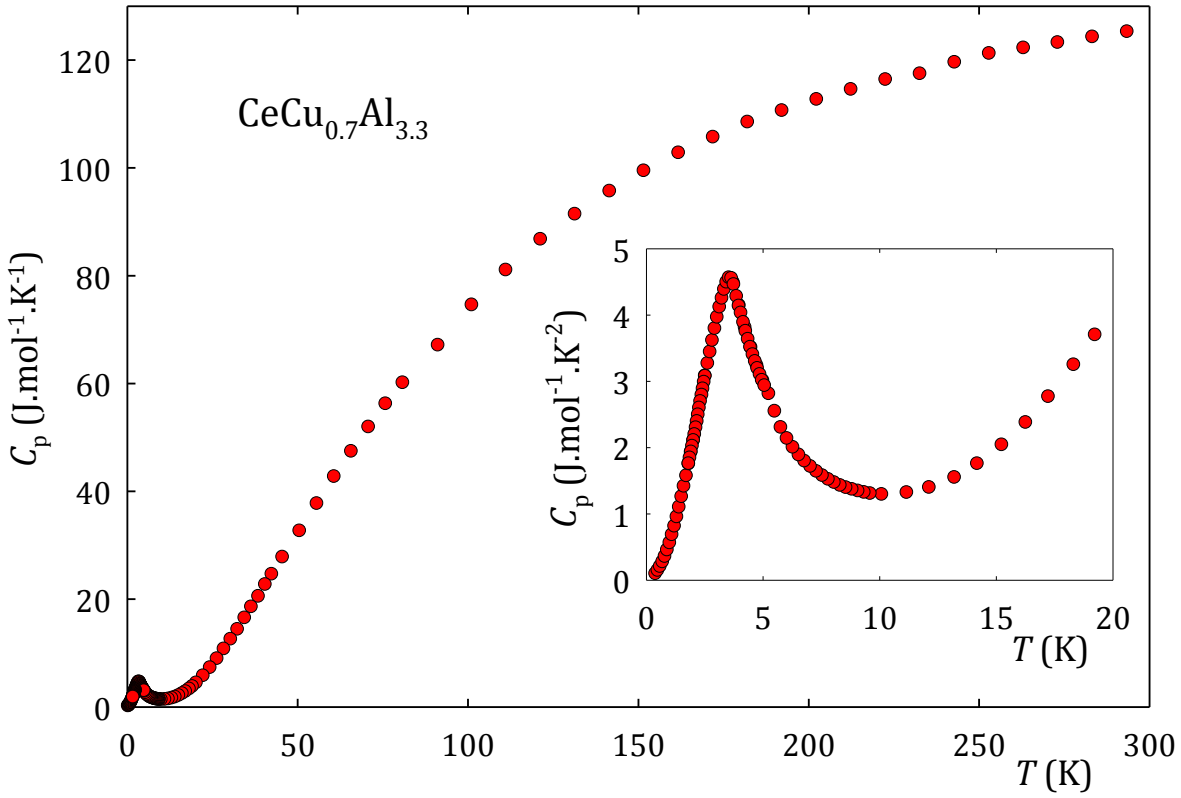

Fig. 19 - Specific heat of $CeCu_{0.7}Al_{3.3}$ in the whole measured temperature range. In the inset is a detail of the same data.

The specific-heat data are presented in Fig. 19. We observe a pronounced anomaly with a maximum around 3.5 K. The shape of this anomaly is typical for a second-order phase transition. The idealization of the specific heat jump under the constraint of entropy conservation yields a magnetic ordering temperature $T_C = (4.0 \pm 0.3)$ K, in agreement with $T_C = 3.7$ K determined from magnetization measurements [47]. The small difference might be due to a slightly different stoichiometry. Upon application of an external magnetic field (see Fig. 20) the entropy moves to higher temperatures, which is indication of ferromagnetic ordering.

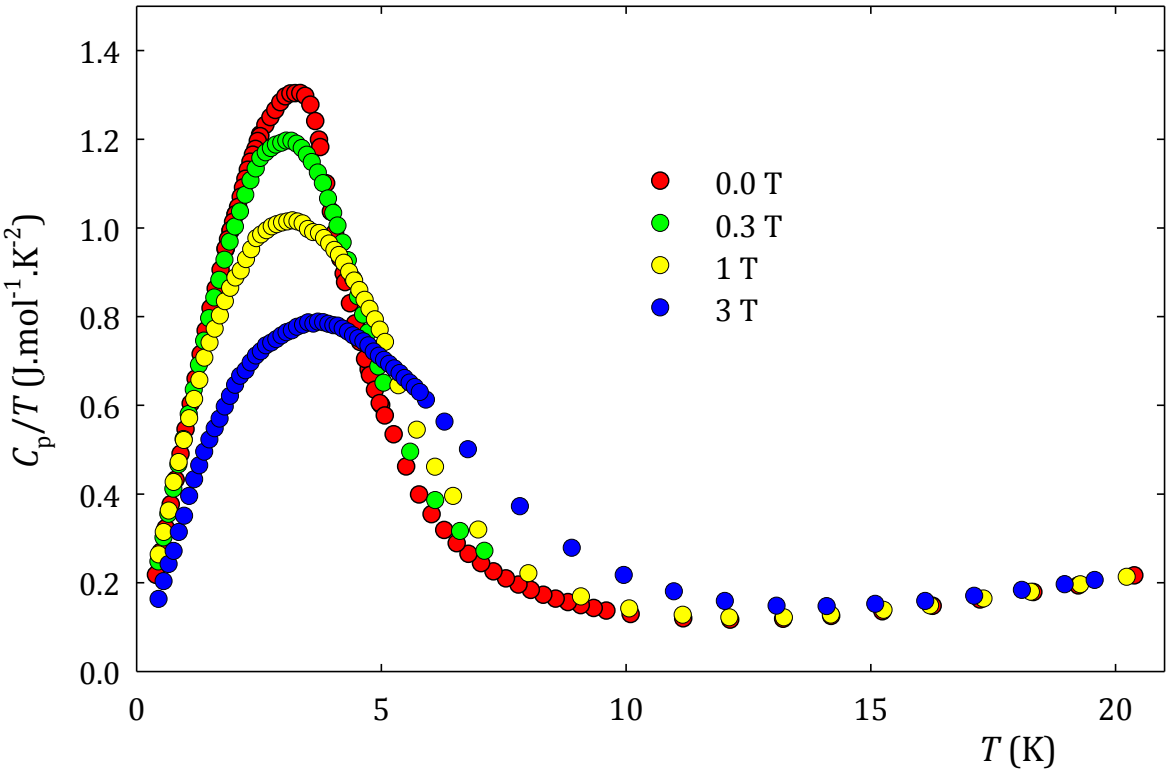

Fig. 20 - C_p/T vs. T dependence for $CeCu_{0.7}Al_{3.3}$ in various magnetic fields.

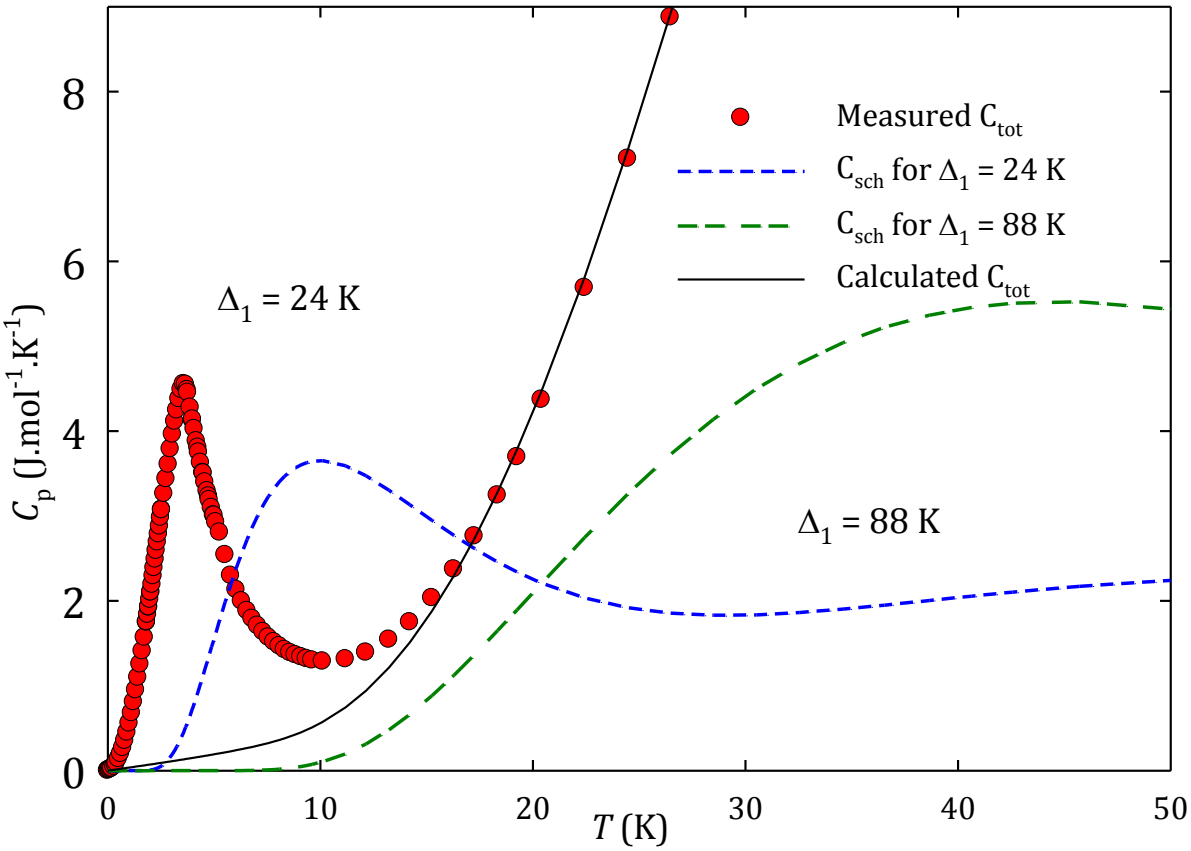

Fig. 21 - Analysis of the Schottky contribution to the specific heat of $CeCu_{0.7}Al_{3.3}$. The dashed lines represent the Schottky contributions calculated for different CF-level splitting. The solid line shows the total specific heat calculated for $\Delta_2 = 88$ K and $\gamma = 35$ mJ.mol^{-1}K^{-2}.

Let us now analyze quantitatively the specific heat in the paramagnetic region. For stoichiometric $CeCuAl_3$, two approaches are found in the literature. Simple extrapolation to 0 K of the linear C_p/T vs. T dependence in the temperature range between 10 and 20 K gives an enhanced γ-coefficient of an electronic specific heat over 100 mJ.mol^{-1}K^{-2} [27] and [28]. In a more realistic approach the relatively small CF splitting between the ground state and the first excited doublet in $CeCuAl_3$ should be considered. An analysis which, besides the electronic and lattice specific heat, also takes into account the Schottky contribution leads to a much smaller γ-value of 24 mJ.mol^{-1}K^{-2} and a CF splitting $\Delta_1 = 13$ K [48], close to the value inferred from magnetization data [29]. We perform a similar analysis of the present $CeCu_{0.7}Al_{3.3}$ sample. First, we consider CF splitting $\Delta_1 = 24$ K and $\Delta_2 = 161$ K as derived from magnetization measurements [47]. The Schottky contribution calculated using these values is represented by the dashed line in Fig. 21. Around 10 K, calculated curve clearly exceeds the total measured specific heat. Thus, we have tried to find CF splittings which is consistent with the presented specific-heat data. Due to absence of a sufficiently precise estimation of the lattice specific heat (e.g. of the non-magnetic analogue $LaCuAl_3$), the overall analysis is rather complicated with a lot of correlated parameters. A reasonable agreement with the experimental data (see Fig. 21) is obtained by assuming Δ_1 to be at least 75 K (values up to $\cong 100$ K are still well acceptable) and a γ-value between 15 and 50 mJ.mol^{-1}K^{-2}, similar to the value of stoichiometric $CeCuAl_3$ [48]. Such a Δ_1 value is three to four times larger than the value resulting from the crystal-field parameters as inferred from magnetization data [47]. To observe the CF excitations directly, neutron scattering experiments would be desirable.

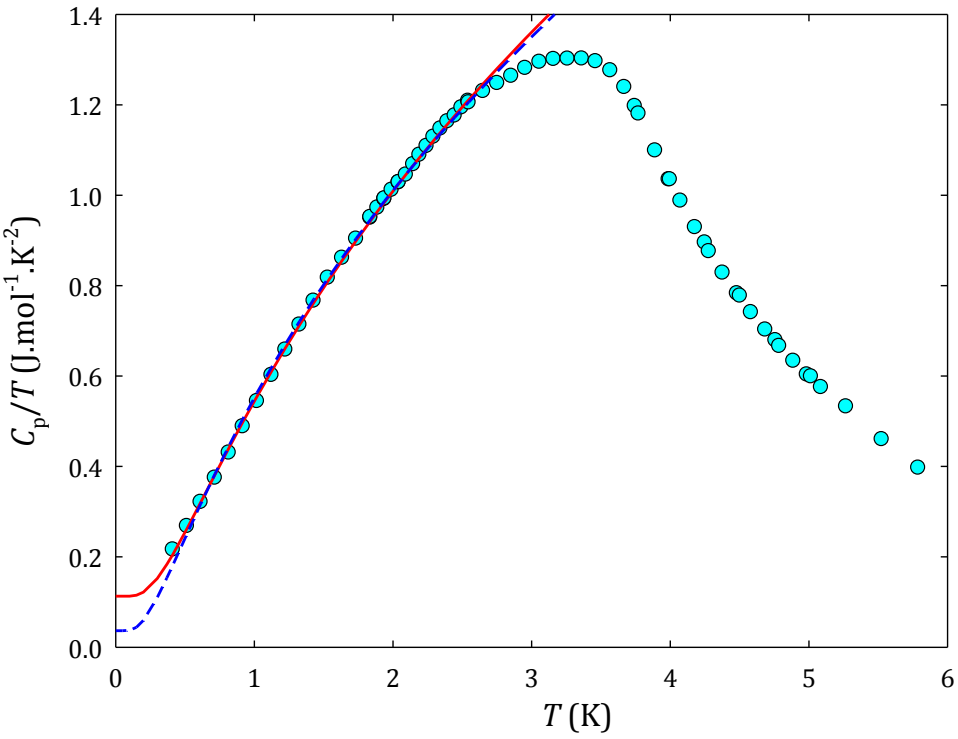

Fig. 22 - C_p/T vs T dependence is shown. The lines represent fits to Eq. (23) (see text for details).

Using a formula (23) and assuming the studied compound to be a three-dimensional ferromagnet (i.e. $d/m = 3/2$), the best agreement with the experimental data between 0.4 and 2.8 K is obtained for $A_{mag} = 0.93$ J.mol^{-1}K$^{-5/2}$, $\gamma = 112$ mJ.mol^{-1}K^{-2} and $\delta = 0.77$ K (full line in Fig. 22). However, the last two obtained parameters are highly correlated and

varying the parameter δ leads to considerable changes of the parameter γ without influencing the quality of the fit. A very good agreement is also obtained for $\gamma = 35$ mJ.mol^{-1}K^{-2}, determined in the paramagnetic region (dashed line in Fig. 22).

The Kondo temperature can be estimated from the value of the molar magnetic entropy S_{mag} at T_C using (19). $S_{mag}(T_c)$ reaches 0.57 Rln2 if considering $\gamma = 35$ mJ.mol^{-1}K^{-2}. Taking into account all uncertainties related to values of γ and T_C, $T_K = 4.0 \pm 0.5$ K was obtained. The Kondo temperature of 4 K is somewhat lower than $T_K = 8$ K estimated for $CeCuAl_3$ [27], but it is different compound (antiferromagnetic). The magnetic entropy then continues to increase in a relatively broad temperature range above T_C up to ~ 10 K, indicating strong magnetic fluctuations even far above T_C. The value of S_{mag} at 14 K amounts 0.92 Rln2, which is near the expected value for a doublet ground state.

4.3. Ce(Ni,Cu)Al

Polycrystalline samples of $CeNi_{1-x}Cu_xAl$ with x = (0; 0.05; 0.1; 0.2; 0.3; 0.5) were prepared by arc-melting stochiometric mixtures of pure elements (4N for Ce, Ni and Cu and 5N for Al). Melting was done under protection of argon atmosphere in a mono-arc furnace. Every sample was turned and re-melted several times to achieve better homogeneity. However samples with higher content of Cu contained impurities. Sample with x = 0.5 contained too large amount of impurities, so it was not used for any further analysis. Samples were not annealed, as recommended in [32], because previous attempts with annealing cause sample decomposition [49]. The refined lattice parameters revealed change of both parameters with increasing x value, see Fig. 23 and Table 1. These values are in agreement with values presented in [50] for pure CeNiAl and CeCuAl.

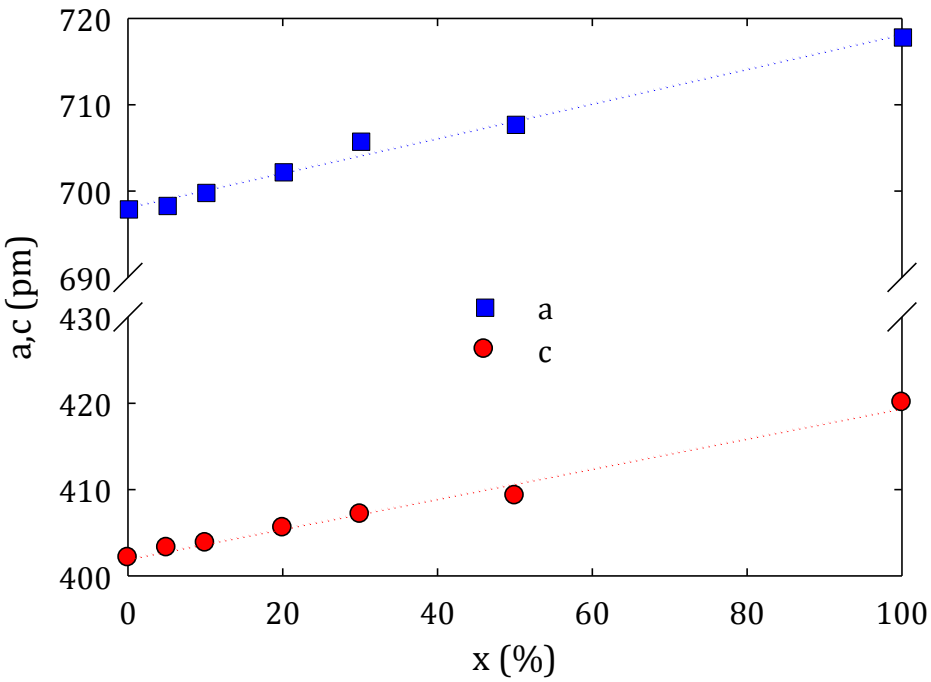

Fig. 23 – Concentration dependence of lattice parameters a and c. Data for CeCuAl was taken from [50]. The dotted lines are to guide the eye.

Table 1 – Refined lattice parameters of $CeNi_{1-x}Cu_xAl$ series

x (%)	a (pm)	c (pm)	V (nm^3)
0	697.0(1)	402.1(1)	0.1697(1)
5	698.4(2)	403.2(1)	0.1703(1)
10	699.9(1)	403.8(1)	0.1713(1)
20	702.3(2)	405.5(1)	0.1732(1)
30	705.8(1)	407.1(1)	0.1757(1)
50	707.8(2)	409.2(1)	0.1776(1)

4.3.1. Magnetization measurements

All samples were first studied by magnetization measurements. Measurements were performed on a MPMS (Magnetic Properties Measurement System) by Quantum Design. The magnetization data were achieved by moving a sample through the superconductive detection coil system, located in the center of the magnet. Change in a magnetic flux causes change of the current in the SQUID detection circuit. Samples were measured under constant field of 2 and 4 T respectively in a temperature range from 10 to 300 K to examine validity of the Curie-Weiss law. Other magnetization measurements were done under constant temperature 1.8 and 5 K respectively to obtain magnetization curves. Applied external magnetic field was up to 7 T.

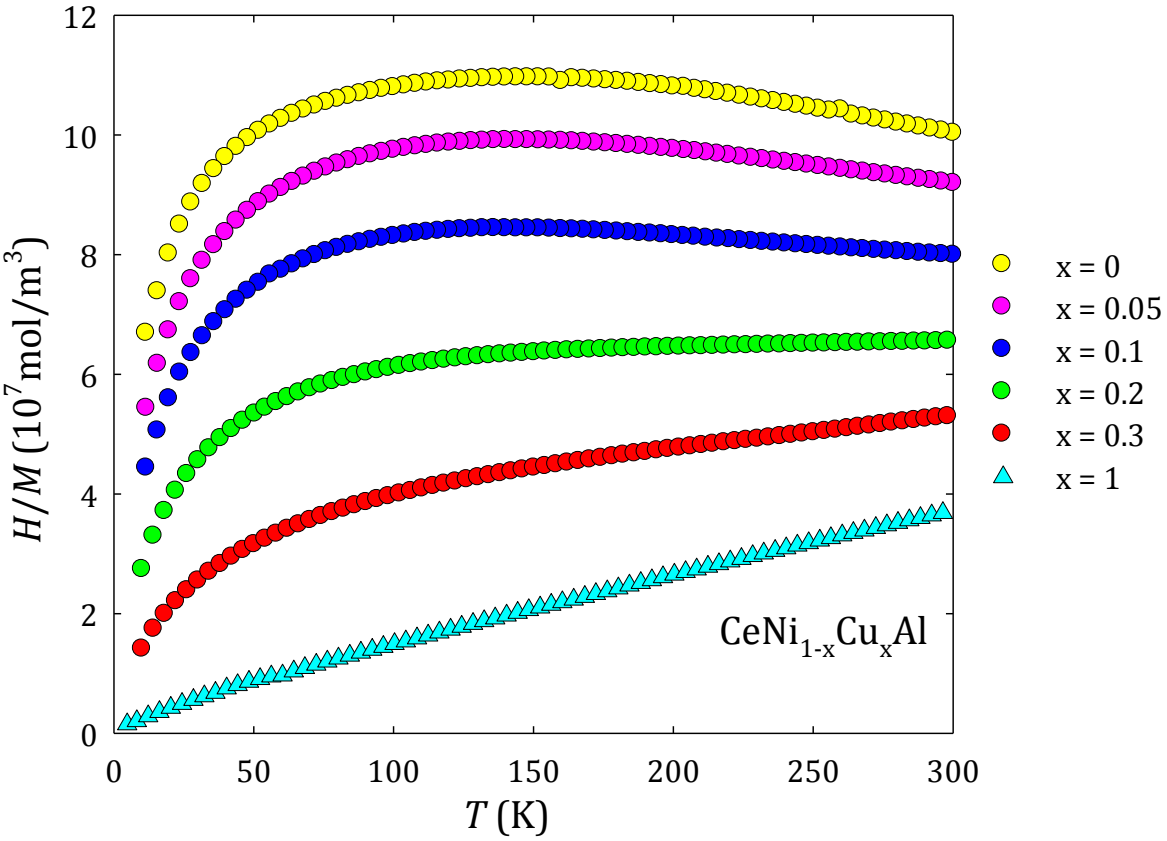

Fig. 24 – $1/\chi\ (T)$ dependences for whole $CeNi_{1-x}Cu_xAl$ series in an external field of 2 T.

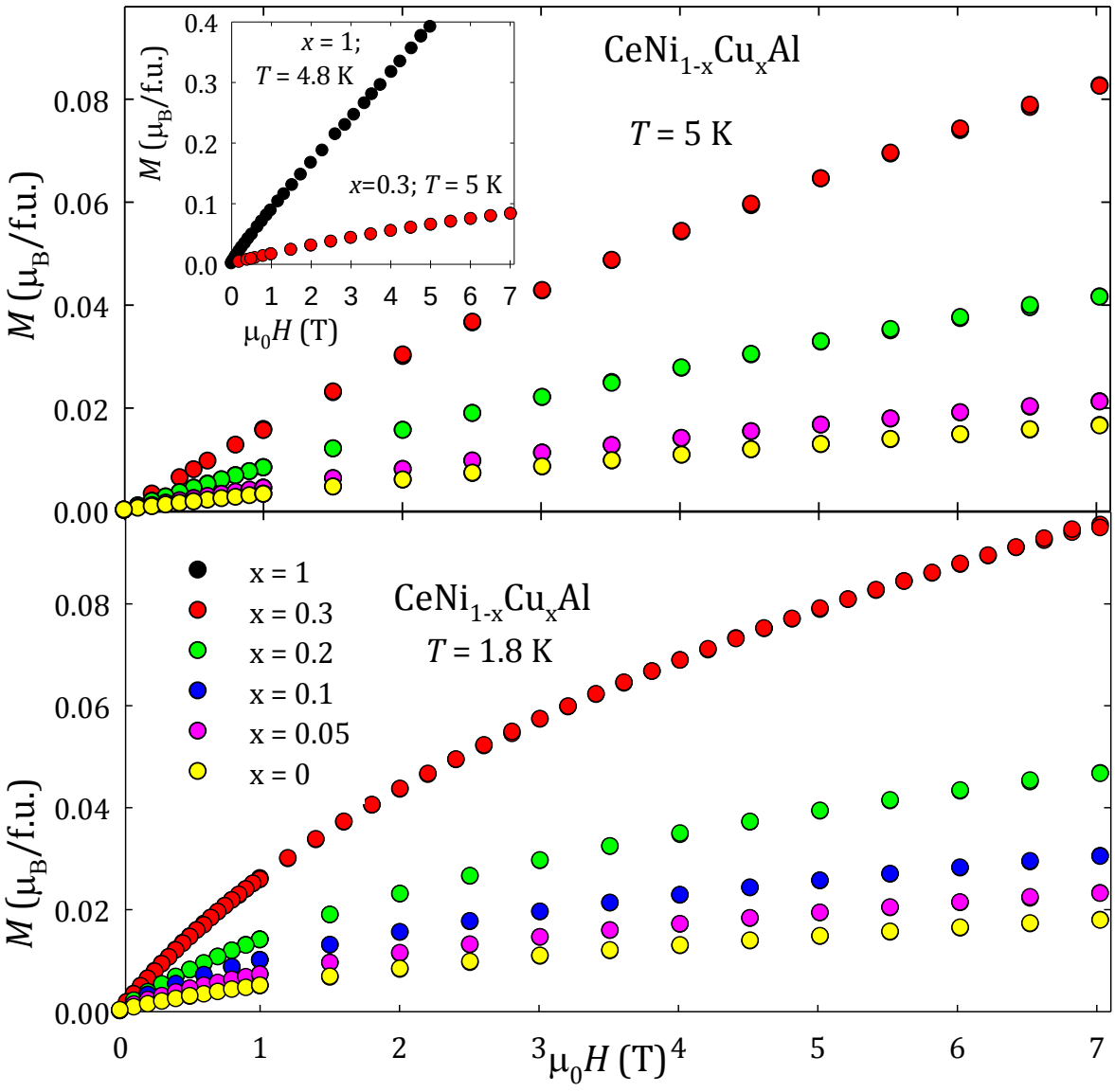

Fig. 25 – Magnetization curves measured at two temperatures (1.8 and 5 K). The inset represents comparison of $CeNi_{0.7}Cu_{0.3}Al$ and CeCuAl measured by Javorský et al. [32]

The Curie-Weiss law gives for a trivalent cerium the theoretical effective moment $\mu_{eff} = 2.54\mu_B$. This value is not generally reached because of various reasons. The value of $\mu_{eff} = 2.18\mu_B$ is reported for the pure CeCuAl, where the lower value of the effective moment is ascribed to nonmagnetic impurities [32]. Anyway, determination of the effective moment as well as paramagnetic Curie temperature θ_p is not possible for our samples, because none of it exhibits Curie-Weiss behavior, indicating mixed valence state. $1/\chi(T)$ dependences for all samples are shown in Fig. 24 together with data measured by Javorský et al. on the pure CeCuAl [32]. We can observer gradual transition from mixed valence to Curie-Weiss behavior, indicated with disappearance of minimum in susceptibility. Applied external magnetic field has no effect to these dependencies so only measurements in the field of 2 T are presented.

Magnetization curves are shown in Fig. 25. They do not exhibit any hysteresis. Very small measured magnetic moments could be explained by mixed valence behavior. We can observe increase of magnetic moments with increasing copper concentration.

4.3.1. Specific heat measurement

The specific heat was measured using a PPMS system in the temperature range between 0.35 and 300 K and in magnetic fields up to 3 T. Small samples with a mass of about 2 mg were measured at temperatures below 5 K and in magnetic fields whereas, in order to archive reasonable precision at higher temperatures where the heat capacity of the sample holder increases considerably, larger samples (~ 20 mg) were used for measurements between 2 and 300 K.

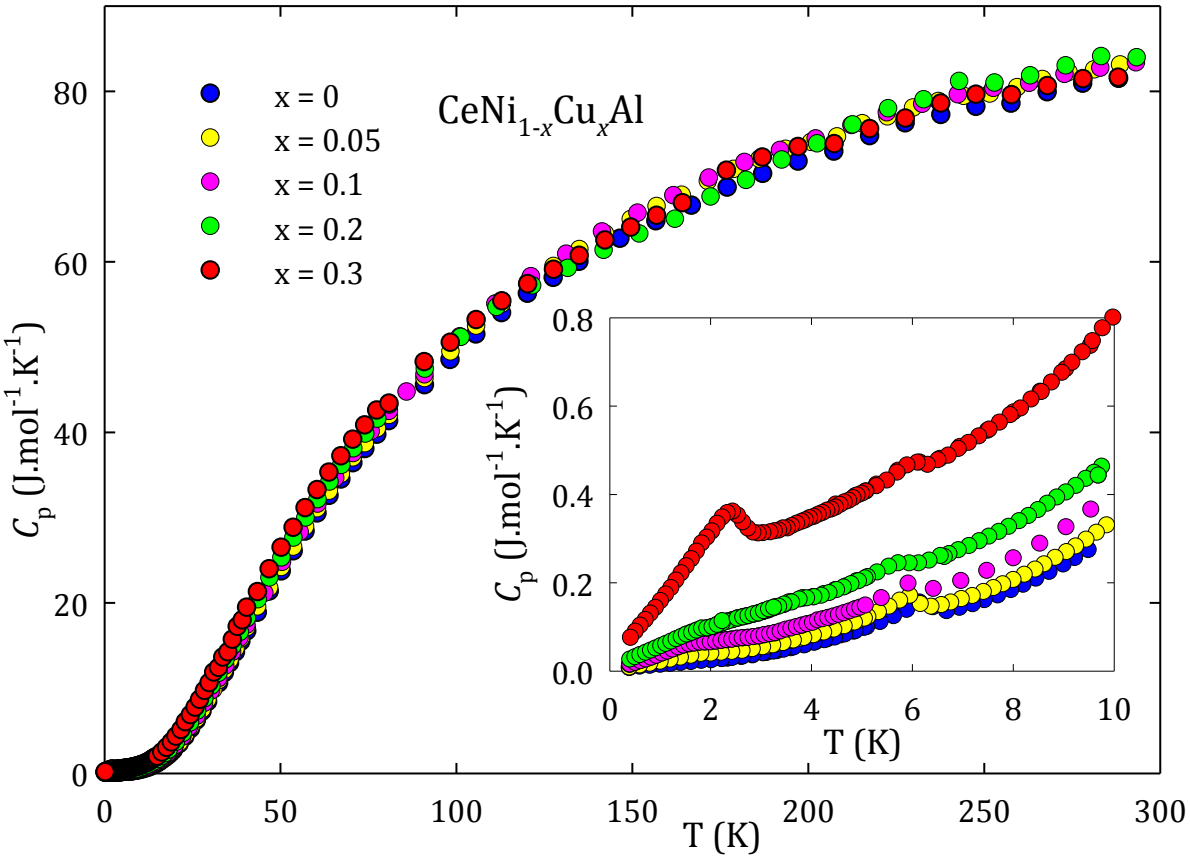

Fig. 26 - The specific heat of the $CeNi_{1-x}Cu_xAl$ compounds in the whole measured temperature range. In the inset is a low temperature detail of the same data.

All measured $C(T)$ dependences are shown in Fig. 26. The data for different compounds are almost the same above 50 K; shift with Cu concentration is only observed in temperature range below 50 K. This signifies that there are no important changes in specific heat contributions along the series in high temperature range. In the low temperature region is observed one small anomaly around 6 K, which can be ascribed to cerium oxide contamination (phase transition at 6.2 K). Bigger anomaly around 2.5 K is observed only for $x = 0.3$, for lower Cu concentration is much reduced. Entropy of this peak is very small ($\approx 5\% \, of \, R \ln 2$) and cannot by exactly calculated, because it interferes very low temperatures, out of the range of PPMS instrument (see Fig. 27).

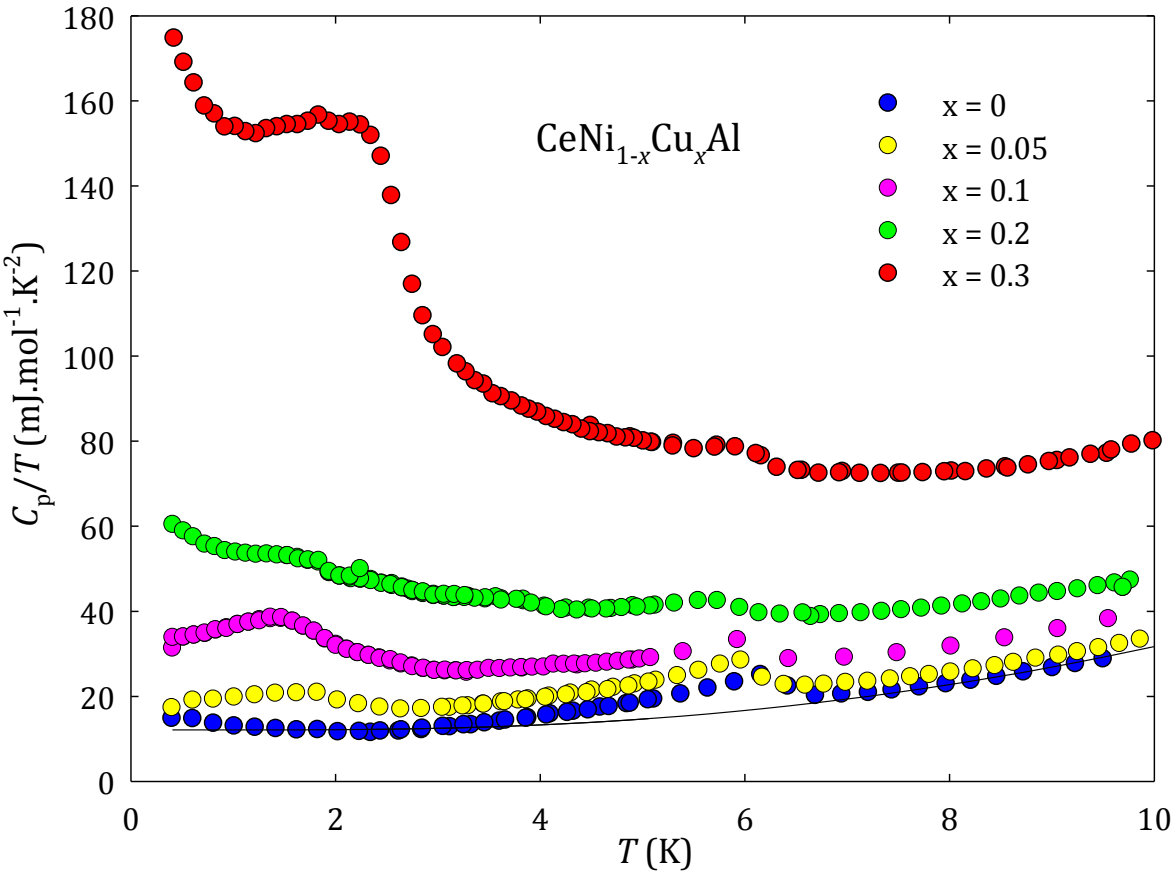

Fig. 27 – $\frac{C}{T}(T)$ dependence for the whole $CeNi_{1-x}Cu_xAl$ series. Solid line is fitted to CeNiAl data, see text for details.

The data below 10 K can be described with equations (10) and (11), which are widely used to describe non-magnetic low temperature specific heat. It can be easily modified to a well known form in which $\frac{C_{LT}}{T}$ is linear function of squared temperature:

$$\frac{C_{LT}}{T} = \gamma + \beta T^2. \tag{24}$$

We must use this relation to fit measured data very carefully. It is valid only in the low temperature range for compounds without magnetic phase transitions or other low temperature excitations. It is possible to use it only for CeNiAl from our series, because with increasing copper concentration there arise excitations from impurities (around 6 K) and also other below 4 K (origin of the entropy arise is uncertain). CeNiAl data evaluation was done accordingly to [32] leading to the same results: $\gamma = 12.1(2)$ mJ.mol^{-1}K^{-2}.

Exact determination of γ-value for other compounds from the series is not possible, but from Fig. 27 is clear that γ-value increases with copper concentration up to ~150 mJ.mol^{-1}K^{-2} as reported for CeCuAl in [32]. This value corresponds to the low temperature linear part of the specific heat. Value of γ_{HT} must be considerably lower, because heat capacity of all measured compounds is almost the same at room temperature (see Fig. 27). See detailed discussion of the similar behaviour of (Ce,Y)PdAl series in 4.1.1. Because electronic specific heat is not linear with temperature, overall analysis of specific heat in a wide temperature range (0-300 K) is quite impossible.

4.4. CePtSn

CePtSn crystallizes in orthorhombic TiNiSi-type structure. It orders antiferromagnetically below $T_N = 7.5$ K. There is another phase transition around 5 K, characterized by appearance of second propagation vector. Our idea was to analyze low temperature specific heat and compare it with other samples.

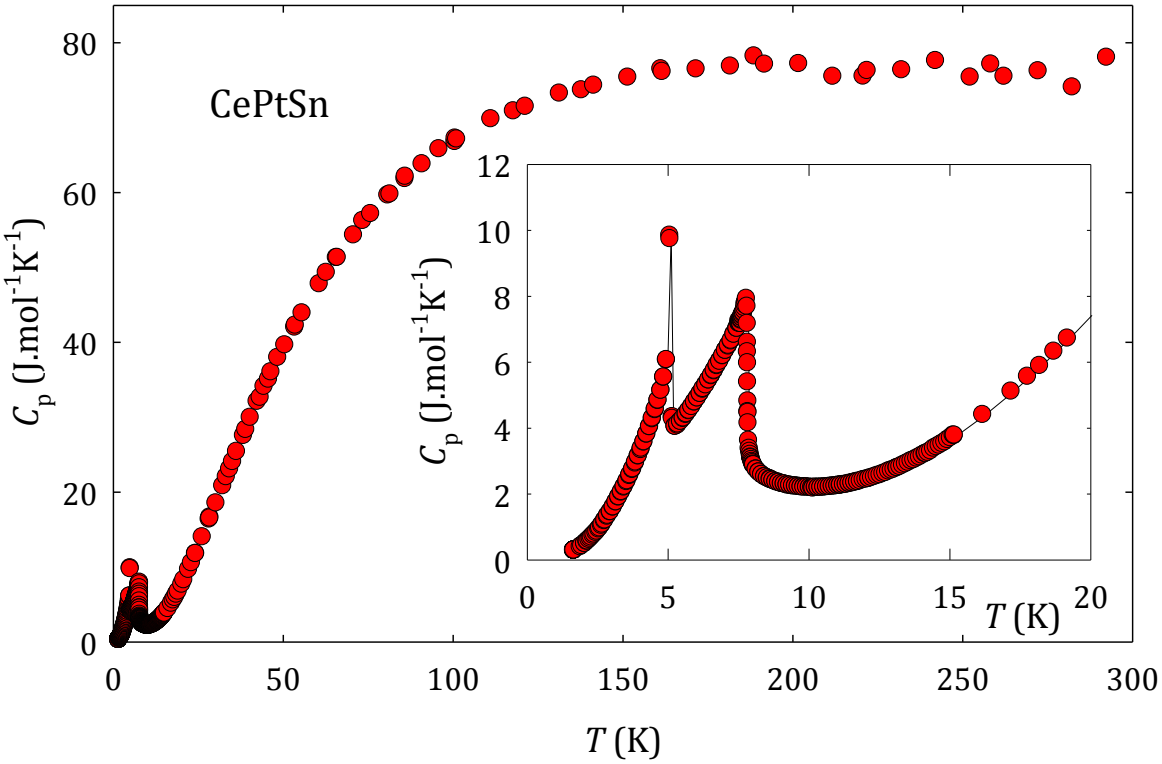

Fig. 28 – Specific heat of CePtSn in the whole temperature range. In the inset is a detail of the low temperature region.

The polycrystalline sample melted by Prokleška et al. [51] was used for the measurements. Specific heat vs. temperature dependence was shown on Fig. 28. Low temperature data below 5 K can be described with (18). Firstly we consider 3-dimensional antiferromagnet without energy gap in a magnon spectra. Fitting function will be:

$$\frac{C_p}{T} = \gamma + A_{mag}\, T^2 \tag{25}$$

and the result leads to $\gamma = 57(4)$ mJ.mol^{-1}K^{-2}. Fitted function is shown in Fig. 29 a). The red line does not exactly follow measured data so one can alternatively consider more complex model. As well as in other cerium compounds, a strong anisotropy of electronic properties is observed in CePtSn. This may exhibit in a decrease of dimensionality d of magnon excitations. To achieve better agreement of fit and measured data, we will use more complex function:

$$\frac{C_p}{T} = \gamma + A_{mag}\, T^{d-1} \exp\left(-\frac{\delta}{T}\right). \tag{26}$$

Result of non-linear least square refinement is shown in Fig. 29 b). The fit leads to $d \cong 2$ and δ between 2 and 3 K. Refined γ-value is the same as the previous one – 61(14) mJ.mol^{-1}K^{-2}, but with considerably higher error.

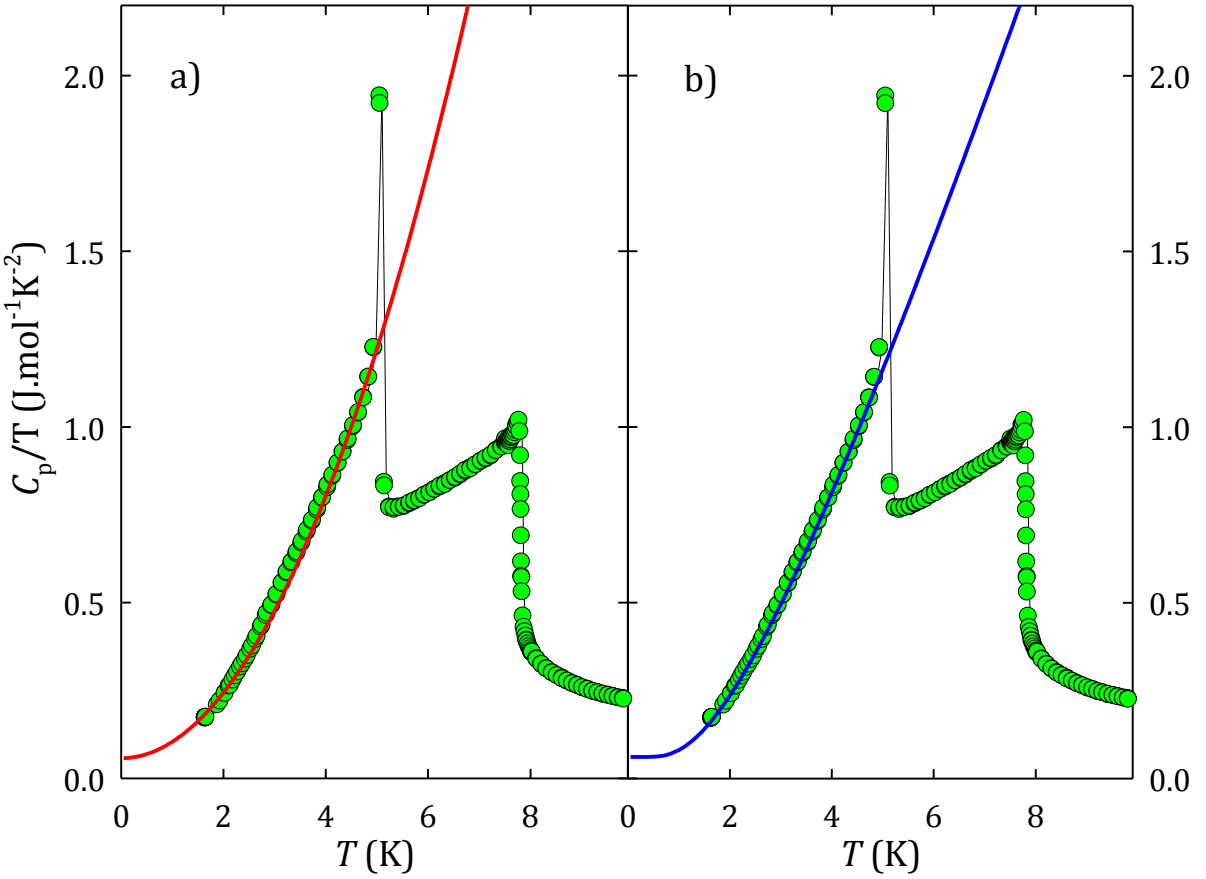

Fig. 29 – Low temperature $\frac{C_p}{T}(T)$ dependence for CePtSn. The left plot a) shows fit with quadratic function (26) and the right plot b) shows more complicated fit to Eq. (27).

4.4.1. Kondo effect

CePtSn is reported to exhibit Kondo behavior with a characteristic Kondo temperature $T_K \cong 10$ K, estimated from the maximum in resistivity [52]. Considering low temperature $\gamma = 60$ mJ.mol^{-1}K^{-2} electronic specific heat can be calculated. Phonon contribution has been assumed to be similar to LaPtSn in low temperatures (up to 15 K). Subtracting these two contributions from measured specific heat C_p we obtain specific heat connected with magnetic transition. Entropy estimation leads to value $S_{mag}(T_N) = 0.68$ Rln2 and total entropy of magnetic transition $S_{mag}(15\ K) = 0.77$ Rln2. Kondo temperature was calculated using equation (19) and the result is $T_K \cong 11$ K which is close to value estimated from resistivity measurements.

4.5. Theoretical models comparison

The main reason of this work was not only to study material properties, but also to compare different specific heat evaluation methods.

4.5.1. Analysis of specific heat related to magnetic order

Three studied compounds have a magnetic phase transition at low temperatures. The CePdAl and the CePtSn exhibit antiferromagnetic order at Néel temperature $T_N = 2.8$ and 7.5 K, respectively. The $CeCu_{0.7}Al_{3.3}$ shows ferromagnetic kind of order at Curie temperature $T_C = 4$ K. All of these compounds can be described with magnetic spin waves theory and we can apply equation (23) to the data region below T_{ord}. In this equation, we have 5 parameters in total, two of them are absolutely correlated. It is parameter d describing dimensionality of the magnon excitations and parameter m describing dispersion relation. Parameter m depends on type of order and thus will not be fitted. A large correlation between γ and the δ parameter was shown on the $CeCu_{0.7}Al_{3.3}$ compound (Fig. 22), so it is questionable to use this fit for determination of the γ-value. Fortunately this correlation applies only for $m = 2$, which means ferromagnetically ordered systems. In the case of CePdAl and CePtSn, parameters are not correlated anymore and the γ-value can be determined relatively precisely. Different fits were done on CePdAl and CePtSn data and it always leads to the same or similar $\gamma - value$. See comparison of all three compounds in Fig. 30.

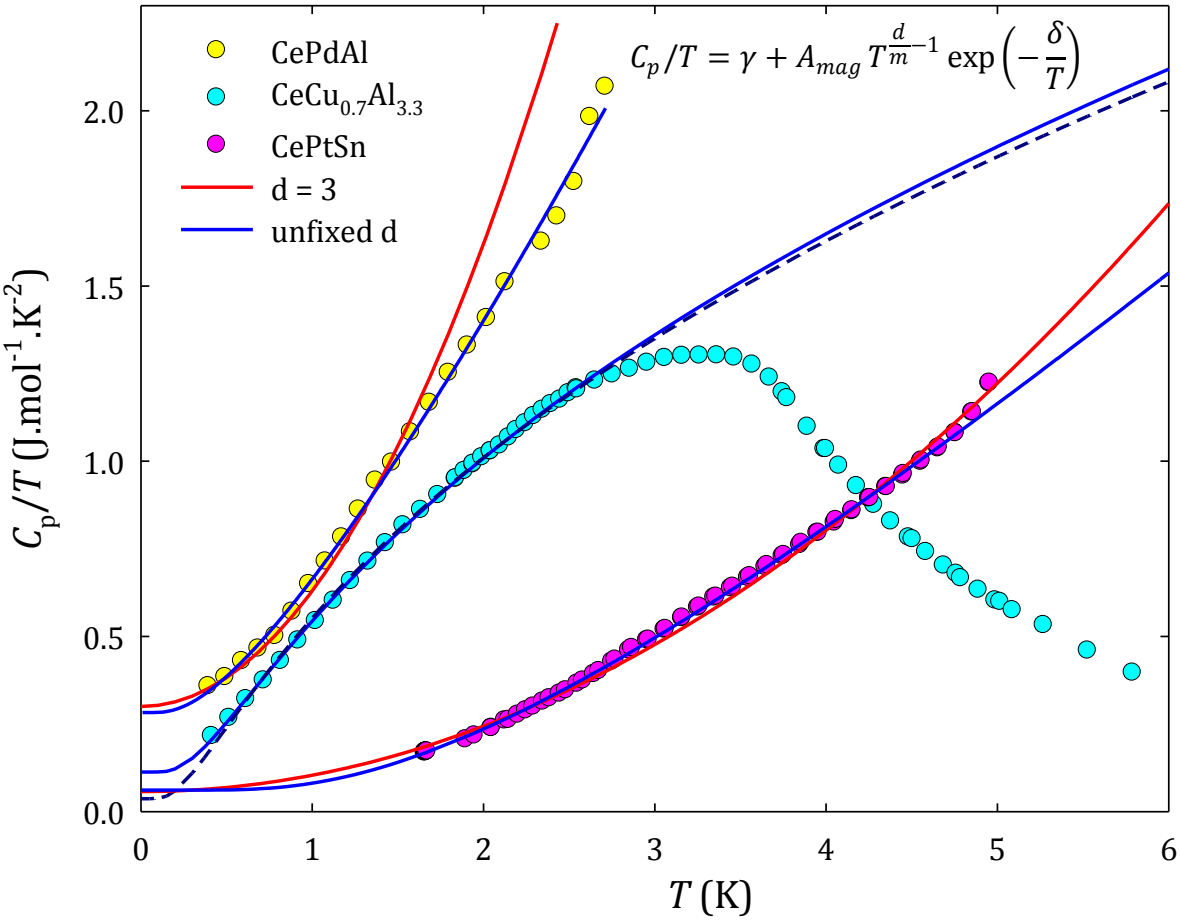

Fig. 30 – Comparison of the application of Eq. (23) on different compounds. Red line represents fit with fixed dimensionality of the system d and blue line represents fit with all four parameters free. Blue dashed line represents alternative fit for $CeCu_{0.7}Al_{3.3}$ which leads to different γ value.

4.5.2. Entropy

As described in the Chapter 2, heat capacity is tightly bound with thermodynamic entropy of the system. If we correctly extract one specific heat contribution, we can easily calculate entropy gain connected with studied phenomena. An entropy connected with magnetic phase ordering was calculated for (Ce,Y)PdAl series, $CeCu_{0.7}Al_{3.3}$ and CePtSn. In the case of a localized Ce^{3+} system with well separated excited crystal field levels, the entropy due to magnetic order should reach the value of $R \ln 2$. In our case, all compounds exhibit Kondo behavior and a magnetic entropy is then reduced. Amount of this reduction is connected with $\frac{T_K}{T_{ord}}$ ratio via equation (19). Despite of very simple model used in equation (19), the results are in a good agreement with other measurements (e.g. electrical resistivity of CePtSn). The position of compound in the Doniach diagram can be determined from the $\frac{T_K}{T_{ord}}$ ratio (see Fig. 31).

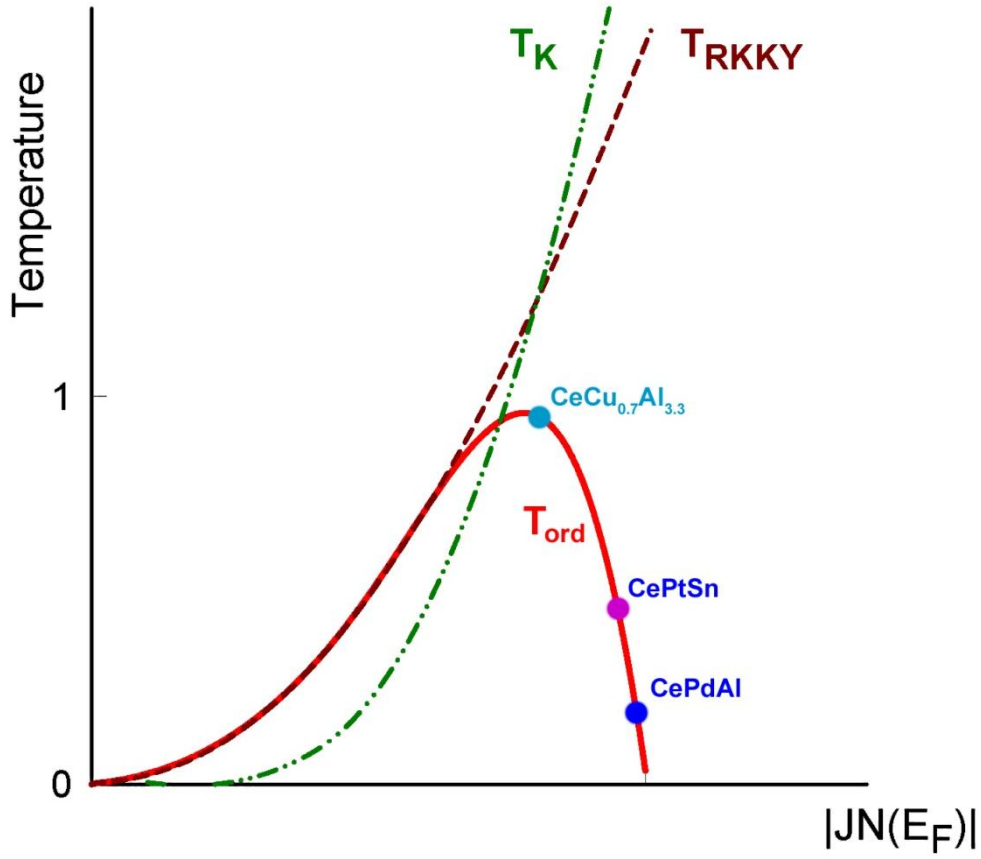

Fig. 31 – Positions of studied Kondo compounds in the Doniach diagram.

5. Conclusion

This thesis was devoted to the measurement and the analysis of the specific heat of selected cerium systems. We have compared application of some simple theoretical models on the complex cerium systems. This models allow us to calculate two important constants characterizing sample: γ-value and Kondo temperature T_K. Comparison of the determined values with the values from other measurement confirms validity of the used simple models.

The specific heat of CePdAl confirms antiferromagnetic order below $T_N = 2.8$ K and is consistent with the metamagnetic phase transition to the ferromagnetic state in applied fields above 4 T. The temperature dependence of the magnetic contribution shows that antiferromagnetic correlations develop from temperatures far above T_N. The ordering temperature decreases rapidly with increasing Y concentration and the magnetic order vanishes around x = 0.2. Also the Kondo temperature decreases with Y concentration. The γ-coefficient of the electronic specific heat shows temperature dependence with a strong increase at low temperatures for all Ce concentrations. The low-temperature limit of the γ-value in CePdAl is close to 300 mJ.mol^{-1}K^{-2} whereas the high-temperature value, that is constant above ~50 K, amounts to only 18 mJ.mol^{-1}K^{-2}. The latter value is only weakly concentration dependent. The neutron diffraction showed that the magnetic structure of the CePdAl does not change significantly with yttrium substitution.

Single crystals of $CeCu_xAl_{4-x}$ were prepared by solution growth from an Al flux. Although this compound exists in a rather broad Cu–Al homogeneity range, the single crystals grown from two different compositions 1:3:16 and 1:2:15 result in the same composition $CeCu_xAl_{4-x}$ with x ~0.7. The specific-heat data confirm ferromagnetic order in this compound below $T_C = 4 \pm 0.3$ K. The first CF energy level lies above 75 K, considerably higher than deduced previously from magnetization measurements. The electronic contribution to the specific heat shows an moderately enhanced Sommerfeld coefficient γ. The Kondo temperature estimated from the value of magnetic entropy at T_C is found to be around 4 K.

We also succeeded in melting of compounds from Ce(Ni,Cu)Al series up to 30% of copper concentrations. The magnetization and specific heat data showed gradual transition from the mixed-valence state in CeNiAl to the Ce^{3+} state in CeCuAl. This development is accompanied by an increase of γ_{LT} with increasing copper content.

The analysis of the specific heat of CePtSn revealed $\gamma_{LT} = 60$ mJ.mol^{-1}K^{-2} and the Kondo temperature $T_K = 11$ K. The latter value is well consistent with previous results of electrical resistivity.

This thesis generally summarizes difficulties of specific heat analysis, forcefully on cerium compounds. We showed that the specific heat data itself do not provide sufficient information about physical properties of given material, and the results from other complementary experimental techniques and/or theoretical calculations is always desirable.

Bibliography

[1] Koskenmaki D. C., Gschneidner J. (1978): Chapter 4 Cerium. *Handbook on the Physics and Chemistry of Rare Earths* **Volume 1**, 337 - 377.

[2] Sereni J. G. (1991): Chapter 98 Low-temperature behaviour of cerium compounds: Specific heat of binary and related intermetallics. *Handbook on the Physics and Chemistry of Rare Earths* **Volume 15**, 1 - 59.

[3] Mackintosh A. R., Jensen J. (1991): Rare Earth Magnetism. Oxford, Clarendon Press.

[4] Martin C. A. (1991): Simple treatment of anharmonic effects on the specific heat. *Journal of Physics: Condensed Matter* **3**, 5967.

[5] Kittel C. (1996): Introduction to solid state physics, 7th ed. New York, John Wiley & Sons.

[6] Sundström L. J. (1978): Chapter 5 Low temperature heat capacity of the rare earth metals. **Volume 1**, 379 - 410.

[7] Blanco J. A., de Podesta M., Espeso J. I., Gómez Sal J. C., Lester C., McEwen K. A., Patrikios N., Rodríguez Fernández J. (1994): Specific heat of CeNixPt1-x pseudobinary compounds and related dilute alloys. *Physical Review B* **49**, 15126.

[8] Bardsley W., Hurle D. TJ., Mullin J. B. (1977): Crystal Growth: A Tutorial Approach. Amsterdam, North-Holland.

[9] Pamplin BR. (1975): Crystal Growth. London, Pergamon Press.

[10] Fisk Z., Remeika JP. (1989): Chapter 81 Growth of single crystals from molten metal fluxes. **Volume 12**, 53 - 70.

[11] Canfield P. C., Fisk Z. (1992): *Philosophical Magazine Part B* **65**, 1117 - 1123.

[12] Canfield P. C., Fisher I. R. (2001): High-temperature solution growth of intermetallic single crystals and quasicrystals. *Journal of Crystal Growth* **225**, 155 - 161.

[13] Wang J., Liu XJ., Wang CP. (2008): Thermodynamic modeling of the Al-U and Co-U systems. *Journal of Nuclear Materials* **374**, 79 - 86.

[14] Hwang J. S., Lin K. J., Tien C. (1997): Measurement of heat capacity by fitting the whole temperature response of a heat-pulse calorimeter. *Review of Scientific Instruments* **68**, 94 - 101.

[15] Hulliger F. (1993): On new ternary aluminides LnPdAl and LnPtAl. *Journal of Alloys and Compounds* **196**, 225 - 228.

[16] Kitazawa H., Matsuhita A., Matsumoto T. (1994): Electronic and thermal properties of CePdAl. *Physica B* **199&200**, 28-30.

[17] Schank C., Jährling F., Luo L., Grauel A., Wassilew C., Borth R., Olesch G., Bredl C. D., Geibel C., Steglich F. (1994): 4f-conduction electron hybridization in ternary Ce-TM-Al compounds. *Journal of Alloys and Compounds* **207/208**, 329-332.

[18] Tang J., Matsushita A., Kitazawa H., Matsumoto T. (1996): High pressure effect on the magnetic transition in heavy fermion systems CePd2Al3 and CePdAl. *Physica B: Condensed Matter* **217**, 97 - 101.

[19] Dönni A., Ehlers G., Maletta H., Fischer P., Kitazawa H., Zolliker M. (1996): Geometrically frustradet magnetic structures of the heavy-fermion compound CePdAl

studied by powder neutron diffraction. *Journal of Physics: Condensed Matter* **8**, 11213-11229.

[20] Keller L., Dönni A., Kitazawa H., van den Brandt B. (2002): Geometrical frustration and incommensurate magnetic ordering in CePdAl: a low-temperature neutron-diffraction study. *Applied Physics A: Materials Science & Processing* **74**, s686 - s688.

[21] Isikawa Y., Mizushima T., Fukushima N., Kuwai T., Sakurai J., Kitazawa H. (1996): Magnetocrystaline Anisotrophy of Magnetic Dense-Kondo Compound CePdAl. *J. Phys. Soc. Jpn.* **65**, Suppl. B 117-122.

[22] Kitazawa H., Prchal J., Tsujii N., Imai M., Kido G. (2006): Magnetic properties of CeYPdAl Kondo-lattice system. *Physica B* **378-380**, 803-804.

[23] Kitazawa H., Tsujii N., Suzuki O., Prchal J., Imai M., Dönni A. (2008): Nonmagnetic La substitution in the geometrically frustrated Kondo system CePdAl. *Physica B: Condensed Matter* **403**, 890 - 892.

[24] Isikawa Y., Kuwai T., Mizushima T., Abe T., Nakamura G., Sakurai J. (2000): Disappearance of magnetic moments in CePd1-xNixAl. *Physica B: Condensed Matter* **281-282**, 365 - 366.

[25] Raghavan V. (2008): Al-Ce-Cu (Aluminum-Cerium-Copper). *Journal of Phase Equilibria and Diffusion* **29**, 264 - 266.

[26] Hu XD., Zhou HY., Li JB., Pan SK., Wang T., Yao QR., Duan LB., Wang YC., Chen XJ., Rao GH. (2009): Phase composition of arc-melted alloys in the ternary systemCe-Al-Cu (Cu-poor portion). *Intermetallics* **17**, 775 - 779.

[27] Bauer E., Pillmayr N., Gratz E., Hilscher G., Gignoux D., Schmitt D. (1987): On the behaviour of the new Kondo lattice CeCuAl3. *Zeitschrift für Physik B Condensed Matter* **67**, 205 - 210.

[28] Lee WH., Yeh MR., Wang DC., Yang FA. (1994): Competition between the screening effect and exchange interactions in the system CeCu1-xAl3+x ($0 \leq x \leq 0.25$). *Japanese Journal of Applied Physics, Part 2: Letters* **33**.

[29] Kontani M., Ido H., Ando H., Nishioka T., Yamaguchi Y. (1994): Magnetic, Transport and Thermal Properties of CeCuAl3 Single Crystal. *Journal of the Physical Society of Japan* **63**, 1652.

[30] Kontani M., Sugihara N., Murase K., Môri N. (1996): High pressure NMR of heavy fermion antiferromagnets CeAl2 and CeCuAl3. *Czechoslovak Journal of Physics* **46**, 2067 - 2068.

[31] Kontani M., Motoyama G., Nishioka T., Murase K. (1999): Magnetic properties of CeCuxAl4-x and CeCuxGa4-x single crystals. *Physica B: Condensed Matter* **259-261**, 24 - 25.

[32] Javorský P., Chernyavsky A., Sechovský V. (2000): Valence fluctuator CeNiAl versus Ce3+ state in CeCuAl. *Physica B: Condensed Matter* **281-282**, 71 - 72.

[33] Chevalier B., Bobet JL. (2001): On the synthesis and physical properties of the intermetallic CeCuAl. *Intermetallics* **9**, 835 - 838.

[34] Rodríguez-Carvajal J. (1993): Recent advances in magnetic structure determination by neutron powder diffraction. *Physica B: Condensed Matter* **192**, 55 - 69.

[35] Javorský P., Havela L., Wastin F., Boulet P., Rebizant J. (2004): Magnetic properties of diluted band ferromagnet URhAl. *Physical Review B* **69**, 054412.

[36] Ślebarski A., Głogowski W., Goraus J., Kaczorowski D. (2008): Magnetic and related properties of the CePd1−xRhxAl system. *Physical Review B* **77**, 125135.

[37] Čermák P. (2008): Analýza magnetického příspěvku k měrnému teplu sloučenin Ce1-xYxPdAl. *Bachelor thesis (in czech).*

[38] Daniel P., Javorský P., Prchal J., Šantavá E., Daniš S. (2007): Lattice heat capacity in RTAl (T = Ni, Cu, Pd) compounds. *Acta physica polonica A* **113**, 331-334.

[39] Moriya T., ru, Takimoto T. (1995): Anomalous Properties around Magnetic Instability in Heavy Electron Systems. *Journal of the Physical Society of Japan* **64**, 960.

[40] Lashley J. C., Singleton J., Migliori A., Betts J. B., Fisher R. A., Smith J. L., McQueeney R. J. (2003): Experimental Electronic Heat Capacities of α- and δ-Plutonium: Heavy-Fermion Physics in an Element. *Physical Review Letters* **91**, 205901.

[41] Ramirez A. P., Espinosa G. P., Cooper A. S. (1992): Elementary excitations in a diluted antiferromagnetic Kagomé lattice. *Physical Review B* **45**, 2505.

[42] Oyamada A., Maegawa S., Nishiyama M., Kitazawa H., Isikawa Y. (2008): Ordering mechanism and spin fluctuations in a geometrically frustrated heavy-fermion antiferromagnet on the Kagome-like lattice CePdAl: A Al27 NMR study. *Physical Review B* **77**, 064432.

[43] Goto T., Hane S., Umeo K., Takabatake T., Isikawa Y. : Field-induced magnetic transitions and pressure-induced magnetic instability in CePdAl. *Journal of Physics and Chemistry of Solids* **63**, 1159 - 1163.

[44] Prokes K., Manuel P., Adroja DT., Kitazawa H., Goto T., Isikawa Y. (2006): Magnetic order in CePdAl single crystal: Effect of magnetic field. *Physica B: Condensed Matter* **385-386**, 359 - 362.

[45] Čermák P., Kitazawa H., Prchal J., Javorský P. (2010): Specific-heat study of the Ce 1 − x Y x PdAl system. *Journal of Physics: Condensed Matter* **22**, 126002.

[46] Stüßer N., Hofmann M. (2002): An adjustable in-pile fan collimator for focusing at a neutron diffractometer. *Nuclear Instruments and Methods in Physics Research Section A: Accelerators, Spectrometers, Detectors and Associated Equipment* **482**, 744 - 751.

[47] Oe K., Kobayashi R., Nishioka T., Kato H., Matsumura M., Kodama K. (2009): Single crystal growth and low temperature magnetic properties of the Ce-Cu-Al ternary system. *Journal of Physics: Conference Series* **150**, 042146.

[48] Mentink S. AM., Bos N. M., van Rossum B. J., Nieuwenhuys G. J., Mydosh J. A., Buschow K. HJ. (1993): Antiferromagnetism and crystal-field effects in CeCuX3 (X=Al,Ga) compounds. *37th Annual conference on magnetism and magnetic materials* **73**, 6625 - 6627.

[49] Javorský P. : private communication.

[50] Oesterreicher H. (1973): Structural and magnetic studies on rare-earth compounds RNiAl and RCuAl. *Journal of the Less Common Metals* **30**, 225 - 236.

[51] Prokleska J., Janousová B., Komatsubara T., Sechovský V. (2005): Thermal expansion and magnetostriction measurements on CePtSn. *Physica B: Condensed Matter* **359-361**,

121 - 123.

[52] Takabatake T., Iwasaki H., Nakamoto G., Fujii H., Nakotte H., de Boer FR., Sechovský V. (1993): Anisotropic effects in the antiferromagnetic Kondo compound CePtSn. *Physica B: Condensed Matter* **183**, 108 - 114.

List of papers containing results of this thesis

Čermák P., Kitazawa H., Prchal J. and Javorský P. (2010): Specific-heat study of the $Ce_{1-x}Y_xPdAl$ system. *Journal of Physics: Condensed Matter* **22**, 126002.

Čermák P., Uhlířová K., Javorský P. (2010): Specific heat of a $CeCu_{0.7}Al_{3.3}$ single crystal, *Physica B: Condensed Matter*, **405**, 2294-2296.